Genome editing of a rice CDP-DAG synthase confers multipathogen resistance

Gan Sha, Peng Sun, Xiaojing Kong, Xinyu Han, Qiping Sun, Laetitia Fouillen, Juan Zhao, Yun Li, Lei Yang, Yin Wang, et al.

Genome editing of a rice CDP-DAG synthase confers multi-pathogen resistance

Gan Sha [1, 13], Peng Sun [1, 13], Xiaojing Kong [1], Xinyu Han [1], Qiping Sun [1], Laetitia Fouillen [2], Juan Zhao [1], Yun Li [1], Lei Yang [1], Yin Wang [1], Qiuwen Gong [1], Yaru Zhou [1], Wenqing Zhou [1], Rashmi Jain [3, 4], Jie Gao [5], Renliang Huang [6], Xiaoyang Chen [1, 12], Lu Zheng [1], Wanying Zhang [1], Ziting Qin [1], Qi Zhou [7], Qingdong Zeng [8], Kabin Xie [5], Jiandi Xu [9], Tsan-Yu Chiu [7], Liang Guo [5], Jenny C. Mortimer [4,10], Yohann Boutté [2], Qiang Li [5], Zhensheng Kang [8], Pamela C. Ronald [3, 4, 11, *], Guotian Li [1, 3, 4, *]

[1]State Key Laboratory of Agricultural Microbiology, Hubei Hongshan Laboratory, Hubei Key Laboratory of Plant Pathology, The Center of Crop Nanobiotechnology, Huazhong Agricultural University, Wuhan, 430070, China

[2]Laboratoire de Biogenèse Membranaire, Univ. Bordeaux, CNRS, Villenave d'Ornon, France

[3]Department of Plant Pathology and the Genome Center, University of California, Davis, Davis, CA 95616, USA

[4]The Joint BioEnergy Institute, Lawrence Berkeley National Laboratory, Emeryville, CA 94608, USA

[5]National Key Laboratory of Crop Genetic Improvement, Huazhong Agricultural University, Wuhan, 430070, China

[6]National Engineering Research Center of Rice (Nanchang), Key Laboratory of Rice Physiology and Genetics of Jiangxi Province, Rice Research Institute, Jiangxi Academy of Agricultural Sciences, Nanchang, 330200, China

[7]BGI-Shenzhen, Shenzhen, Guangdong, 518083, China

[8]State Key Laboratory of Crop Stress Biology for Arid Areas, Northwest A&F University, Yangling, 712100, China

[9]Institute of Wetland Agriculture and Ecology, Shandong Academy of Agricultural Sciences, Jinan 250100, China

[10]School of Agriculture, Food and Wine, University of Adelaide, Glen Osmond, SA, Australia

[11]Innovative Genomics Institute, University of California, Berkeley, Berkeley, CA 94704, USA

[12]Present address: College of Plant Protection, Anhui Agricultural University, Hefei, 230036, China

[13]These authors contributed equally: Gan Sha and Peng Sun.

*Address correspondence to pcronald@ucdavis.edu (Pamela C. Ronald) and li4@mail.hzau.edu.cn (Guotian Li).

The discovery and application of genome editing introduce a new era of plant breeding, giving researchers efficient tools for the precise engineering of crop genomes[1]. Here, we demonstrate the power of genome editing for engineering broad-spectrum disease resistance in rice (*Oryza sativa*). We first isolated a lesion mimic mutant (LMM) from a mutagenized rice population, demonstrated that a 29-bp deletion in a gene we named *RESISTANCE TO BLAST1* (*RBL1*) caused this phenotype and showed that this mutation caused a ca. 20-fold reduction in yield. *RBL1* encodes a cytidine diphosphate diacylglycerol (CDP-DAG) synthase required for phospholipid biosynthesis[2]. Mutation of *RBL1* results in reduced levels of phosphatidylinositol (PI) and its derivative PI(4,5)P_2. Rice PI(4,5)P_2 is enriched in cellular structures specifically associated with effector secretion and fungal infection, suggesting a role as a disease susceptibility factor[3]. Using targeted mutagenesis, we obtained an allele of *RBL1,* named *RBL12,* which confers broad-spectrum resistance but does not decrease yield in a model rice variety as assessed in small-scale field trials. Our study has demonstrated the usefulness of editing of an LMM gene, a strategy relevant to diverse LMM genes and crops.

Main text

Genome editing has been widely used in functional studies of genes but its potential for crop improvement has not yet been broadly utilized[4]. Plant diseases cause severe losses in agriculture, threatening global food security[5]. Rice blast alone, caused by the fungal pathogen *Magnaporthe oryzae,* results in annual yield losses that are sufficient to feed more than 60 million people worldwide[6]. Given this cost, cultivating crops with resistance to diseases, particularly broad-spectrum resistance, is highly desirable[7]. Despite the importance of this goal, only a limited number of broad-spectrum resistance genes have been cloned and used in the field, such as rice *Xa21* (ref.[8])*, bsr-d1* (ref.[9]), *Pigm*[10], *IPA1* (ref.[11]), *ROD1* (ref.[12]), *UMP1* (ref.[13]), wheat *Lr34* (ref.[14]) and *PsIPK1* (ref.[15]), and barley *mlo*[16,17].

LMMs form hypersensitive response-like lesions (a form of programmed cell death) in the absence of pathogens[18]. LMMs often confer durable and broad-spectrum resistance, representing a potential source for breeding resistance to diseases. However, LMMs are usually associated with reduced yield, and therefore the use of the genes conferring LMM phenotypes (hereafter referred to as LMM genes) has not been fully exploited in plant breeding due to the lack of useful alleles.

Phospholipids are essential components of biological membranes and are involved in various biological processes, including development and response to biotic and abiotic stress[19]. In phospholipid biosynthesis (Extended Data Fig. 1), phosphatidic acid (PA) and cytidine triphosphate (CTP) are converted to CDP-DAG by CDP-DAG synthases (CDSs). CDP-DAG and *Myo*-inositol are used to produce PI by phosphatidylinositol synthases (PISs)[20]. PI is added to by a varied number of phosphate groups to synthesize different phosphatidylinositolphosphates (PIPs), including PI3P, PI4P and PIP_2. In

particular, plant PI(4,5)P_2 has been demonstrated to be a disease susceptibility factor[3,21]. The role of phospholipids in rice immunity is largely unknown.

Mutant *rbl1* shows enhanced immunity

To identify new LMM genes, we visually screened over 1,500 whole-genome sequenced fast-neutron mutagenized lines in the rice variety Kitaake[22]. One of the six identified LMMs, named *rbl1,* was of particular interest because it showed enhanced resistance to both *Xanthomonas oryzae* pv. *oryzae* (*Xoo*) and *M. oryzae* (Fig. 1a-f), though low in fertility (Extended Data Fig. 2a). The infection rate (3.4%) of *M. oryzae* appressoria in *rbl1* is significantly reduced compared to that (79.8%) Kitaake infected plants (Fig. 1g). Fungal hyphae spread restrictively in *rbl1* compared to Kitaake at 72 hours post-inoculation (hpi), possibly because the fungus triggers the accumulation of reactive oxygen species (ROS) in *rbl1* (Fig. 1h, i). Similarly, *rbl1* showed significant upregulation of ROS, salicylic acid accumulation, and plant defense-related genes (Extended Data Fig. 2b-d). These responses have previously been observed in other LMMs, including *EBR1* (ref.[23]), *spl-D*[24] and *oscul3a*[25].

Genetic analysis of a segregating M3 population of *rbl1* revealed that the lesion mimic phenotype is controlled by a recessive locus (Extended Data Fig. 2e). Subsequently, we whole-genome sequenced pooled DNA from three lesioned M3 segregants using Illumina[22] and identified a 29-bp deletion in *RBL1* (LOC_Os01g55360) (Fig. 1j). The deletion cosegregated with the LMM phenotype. The deletion overlaps the ninth exon-intron junction in gene *RBL1* and causes an inframe deletion of the ninth exon, resulting in a 19-amino acid truncation at the conserved C-terminus of RBL1 (ref.[26]) (Fig. 1k, l). The truncation overlaps the CDS signature motif for ion-binding[27], likely resulting in loss of function for RBL1. The genetic complementation assays confirmed that *RBL1* is the causative gene (Fig. 1m-p, and Extended Data Fig. 2f-g). Additionally, *RBL1* is transcribed in all examined tissues with the highest level in leaf, and its expression was induced by *M. oryzae* infection (Extended Data Fig. 3).

RBL1 synthesizes CDP-DAG, a PI precursor

As *RBL1* homologs are well conserved (Extended Data Fig. 4a-c), we used heterologous expression to study its biochemical function using the yeast *cds1* mutant (Fig. 2a). The *RBL1* gene driven by a galactose-inducible promoter was transformed into the *cds1* mutant. The resultant yeast strain cdsC grew well on the galactose-containing media but not glucose-containing media, and RBL1 forms a homodimer in yeast (Fig. 2b). Using lipidomics analysis, we detected higher levels of PA and DAG, and reduced levels of PI and phosphatidylglycerol (PG) in the yeast cells cultured in the glucose-containing media compared to those in the galactose-containing media (Fig. 2c). These results suggest that RBL1 functions as a CDP-DAG synthase.

We next used lipidomics technology to investigate the function of *RBL1* in rice. Levels of PA and DAG in *rbl1* are higher than levels observed in Kitaake. In contrast, levels of PI and PG were reduced

significantly by 71% and 49%, respectively (Fig. 2d). The reduction in PI is the most striking result of the phospholipid alterations (Fig. 2e). To test whether exogenous supplementation of phospholipids could rescue the LMM phenotype, we performed chemical complementation assays and observed that exogenous supplementation of the media with PI but not PG, or $PI(4,5)P_2$ postponed lesion formation in *rbl1*, whereas PA accelerated lesion formation (Extended Data Fig. 5a-d). As respiratory burst oxidase homolog (RBOH) proteins are important for ROS generation[28], we applied the RBOH inhibitor-diphenyleneiodonium chloride (DPI) to *rbl1*. We observed that DPI could alleviate the LMM phenotype (Extended Data Fig. 5e).

To test whether increased production of PI could rescue the LMM phenotype, we overexpressed *OsPIS1* in *rbl1*. These *OsPIS1* overexpression lines (OPIS1::*rbl1*) accumulated 60- to 400-fold higher levels of *OsPIS1* transcript than in *rbl1* (Supplementary Fig. 1). Compared to *rbl1*, lesion formation in the OPIS1::*rbl1* lines was alleviated (Fig. 2f-h). Consistent with these results, *PR* gene expression and resistance to *M. oryzae* in the OPIS1::*rbl1* plants are lower than levels observed in *rbl1* but higher than levels in Kitaake (Fig. 2i, j). The PI content of the OPIS1::*rbl1* plants (0.817 nmol mg^{-1} DW) was restored to 80% of that in Kitaake (1.017 nmol mg^{-1} DW), a significant increase from the *rbl1* line (0.319 nmol mg^{-1} DW, $P < 0.01$). We further analyzed PIP and PIP_2 content and observed that their levels were fully restored in OPIS1::*rbl1* lines from the reduced levels in *rbl1*, though the disease susceptibility was only partially restored (Fig. 2k). Similarly, we overexpressed the PA phosphohydrolase-encoding gene *OsPAH2* in *rbl1* (Fig. 2l). However, the OPAH2::*rbl1* line, while restored in PA content, only shows a minor reduction in the expression levels of *PR* genes and no alteration in lesion formation or resistance to *M. oryzae* (Fig. 2m-o), indicating that elevated PA levels in *rbl1* only contribute to enhanced immunity in a limited way. Thus, we focused on PI derivatives in subsequent studies.

$PI(4,5)P_2$ in infection-specific structures

Using lipid blotting with PIP_2-specific antibodies, we showed the reduction of membrane $PI(4,5)P_2$ in *rbl1* (Fig. 3a, b). To further analyze the spatiotemporal changes of $PI(4,5)P_2$ *in situ* during fungal infection, we generated stable transgenic rice lines expressing the $PI(4,5)P_2$ biosensor. $PI(4,5)P_2$ distributes evenly along the plasma membrane in Kitaake. In contrast, $PI(4,5)P_2$ shows weak signals in the plasma membrane and is present in unknown intracellular vesicles in *rbl1* (Fig. 3c). Consistent with the western blotting results, membrane $PI(4,5)P_2$ is reduced in *rbl1* compared to Kitaake based on fluorescence signals (Fig. 3d, e). Upon infection by *M. oryzae*, $PI(4,5)P_2$ quickly aggregates at the invasive hyphal tip like a cap (Fig. 3f). As fungal infection progresses, $PI(4,5)P_2$ is recruited to the extra-invasive hyphal membrane (EIHM) that encapsulates fungal infectious hyphae (Fig. 3g, h). Specifically, $PI(4,5)P_2$ is enriched in an infection-specific structure called the biotrophic interfacial complex (BIC)-indicated by the fluorescent cytoplasmic effector Pwl2 (Fig. 3i), which is important for effector secretion and fungal

infection[29]. PI(4,5)P_2 was hardly observed in the cytoplasm of *rbl1*. The BIC formation rate is only 16.7% in *rbl1* in contrast to 93.3% in Kitaake (Fig. 3j). Taken together, these results suggest that PI(4,5)P_2 could play a role in fungal-rice interactions (Fig. 3k).

RBL12 balances growth and immunity

The *rbl1* line displays broad-spectrum resistance but shows a ca. 20-fold reduction in yield (Extended Data Fig. 2a). To further evaluate the effects of different *RBL1* alleles on plant yield and immunity, we designed guide RNAs by targeting multiple sites in *RBL1* using a multiplexing genome editing strategy (Fig. 4a and Extended Data Fig. 6a-d). We obtained a total of 57 T0 edited lines; 38 of these showed obvious LMM phenotypes and reduced seed sets, similar to *rbl1*. Nineteen of the edited lines displayed no or fewer lesions and varied seed sets in the greenhouse (Fig. 4b). Notably, the *RBL12* line with a 12-bp deletion, which only showed tiny hypersensitive response-like lesions starting at the booting stage (Fig. 4c, Extended Data Fig. 7a and Supplementary Fig. 2), produced a normal seed set (Fig. 4d). Detailed infection assays revealed that *RBL12* conferred resistance to 10 *M. oryzae* field strains, 5 *Xoo* strains, and 2 rice false smut *Ustilaginoidea virens* strains (Fig. 4e-j). Accordingly, levels of mycotoxins in infected spikelets by *U. virens* are reduced by 66.2% in *RBL12* compared to that in Kitaake (Fig.4i). We next carried out small-scale field trials aimed at assessing the usefulness of *RBL12* with transgene-free seeds (Extended Data Fig. 6e-g). The grain yield of *RBL12* was evaluated in four fields in three provinces (18°41'-30°47' N), primary rice production areas of China, where no or little *M. oryzae* was present. Multiple key agronomic traits including plant height, tiller number per plant, seed setting rate, thousand-grain weight, and grain yield were assessed. We found that, except for plant height, all measured traits were similar between *RBL12* and Kitaake (Extended Data Fig. 6h). *RBL12* yielded 1.66 kg of grains per hundred plants, compared to 1.70 kg of grains for Kitaake (Fig. 4k). In a fifth location (Enshi) with a high incidence of *M. oryzae*, the *RBL12* plants displayed robust resistance to both leaf and panicle blast. The panicle blast severity of *RBL12* was 15.8%, much lower than that of Kitaake, which was 90.3%. Regarding yield, we found that *RBL12* yielded 5.3-fold more grains than the control Kitaake plants that were severely damaged by blast (0.75 vs. 0.12 kg per hundred plants) (Fig. 4l, m). Taken together, these results demonstrate that the *RBL12* allele in Kitaake confers robust broad-spectrum disease resistance with no reduction in yield in a small-scale field trial.

We next analyzed the *RBL12* allele in detail. The four amino acids truncated in RBL12 are conserved in plants (Extended Data Fig. 7b). The increased level of ROS in *RBL12* when challenged with chitin is within the range of other rice cultivars (Extended Data Fig. 7c). The 12-bp deletion causes a significant reduction in gene expression, though no alteration in protein thermostability and subcellular localization was observed (Extended Data Fig. 7d-i). *RBL1* complements the *RBL12* line but the *RBL12* allele does not complement *rbl1* (Extended Data Fig. 7j-l). The complementation result was confirmed in the F2

population derived from Kitaake crossed with *RBL12*, which also indicates that the *RBL1* locus contributes to resistance in a reverse dosage-dependent manner (Extended Data Fig. 7m-o). The PIP_2 levels and BIC formation rate are reduced in the *RBL12* line compared with Kitaake (Extended Data Fig. 7p-s). These results indicate that the *RBL12* allele results in a four-amino acid truncation and a reduction in *RBL12* gene expression. We have also generated *RBL1* edited lines in two other rice cultivars, Nipponbare and Zhonghua11, and observed enhanced resistance to *M. oryzae* and normal growth, similar to *RBL12* (Extended Data Fig. 8).

Discussion

These results reveal a connection between rice phospholipid metabolism and rice immunity. They further indicate important functions of RBL1, a CDP-DAG synthase, in the control of programmed cell death and immunity via the regulation of PI biosynthesis. In Arabidopsis, the knockdown *cds* mutants show enhanced immunity (Extended Data Fig. 4d-i)[30]. These results suggest that *RBL1* homologs play conserved roles in immunity. A recent study shows that mutation of *OsCDS5* enhances tolerance of rice to hyperosmotic stress[31]. Taken together, these results suggest that CDSs play broad roles in plant biotic and abiotic stress responses. PI derivatives play crucial roles in biology[32]. Of the PI derivatives, the $PI(4,5)P_2$ level is reduced both in *rbl1* and *RBL12.* Recently, PIP and PIP_2 were demonstrated to be involved in plant and animal immunity[33-35]. Our results specifically show that $PI(4,5)P_2$ is enriched in the BIC and EIHM (Fig. 3i), structures involved in effector secretion and *M. oryzae* infection[29]. This observation is consistent with studies that report $PI(4,5)P_2$ serves as a disease susceptibility factor that is recruited to infection sites to facilitate infection[3,21]. The exact role of $PI(4,5)P_2$ and PIP in fungal effector secretion, rice immunity, and the relevant regulatory mechanisms[36] need further investigation. Through genome editing, the *RBL12* allele in a model rice variety confers broad-spectrum resistance but does not reduce yield in small-scale field trials. The results reported here suggest that fine-tuning of host factors involved in formation of infection-specific structures is a strategy for balancing immunity and yield. Our observations of the performance of the *RBL12* plants are promising. Multi-year field trials are needed to evaluate the performance of the *RBL12* allele in elite, locally adapted rice varieties.

Like the atypical *R* genes *Lr34* and *mlo, RBL1* was isolated from LMMs. *Lr34* and *mlo* are well conserved and have been applied to multiple crops for disease resistance[37,38]. Similarly, the *RBL1* homologs in other crops are worthy of further investigation. LMM genes, often encoding negative regulators of immunity, represent an important class of genes conferring broad-spectrum resistance[7,39]. Negative regulators are particularly compatible with genome editing technologies that can efficiently create complete or partial loss-of-function alleles[40,41]. With continued advances of genome editing technologies[1], the strategy demonstrated in this study becomes increasingly valuable to diverse LMM genes and crops.

205 **References**

206 1 Gao, C. Genome engineering for crop improvement and future agriculture. *Cell* **184**, 1621-1635
207 (2021).
208 2 Liu, X., Yin, Y., Wu, J. & Liu, Z. Structure and mechanism of an intramembrane liponucleotide
209 synthetase central for phospholipid biosynthesis. *Nat. Commun.* **5**, 4244 (2014).
210 3 Qin, L. *et al.* Specific recruitment of phosphoinositide species to the plant-pathogen interfacial
211 membrane underlies *Arabidopsis* susceptibility to fungal infection. *Plant Cell* **32**, 1665-1688 (2020).
212 4 Zhu, H., Li, C. & Gao, C. Applications of CRISPR-Cas in agriculture and plant biotechnology. *Nat.*
213 *Rev. Mol. Cell Biol.* **21**, 661-677 (2020).
214 5 Chen, K., Wang, Y., Zhang, R., Zhang, H. & Gao, C. CRISPR/Cas genome editing and precision
215 plant breeding in agriculture. *Annu. Rev. Plant. Biol.* **70**, 667-697 (2019).
216 6 Sakulkoo, W. *et al.* A single fungal MAP kinase controls plant cell-to-cell invasion by the rice blast
217 fungus. *Science* **359**, 1399-1403 (2018).
218 7 Li, W., Chern, M., Yin, J., Wang, J. & Chen, X. Recent advances in broad-spectrum resistance to
219 the rice blast disease. *Curr. Opin. Plant Biol.* **50**, 114-120 (2019).
220 8 Song, W. Y. *et al.* A receptor kinase-like protein encoded by the rice disease resistance gene, *Xa21*.
221 *Science* **270**, 1804-1806 (1995).
222 9 Li, W. *et al.* A natural allele of a transcription factor in rice confers broad-spectrum blast resistance.
223 *Cell* **170**, 114-126.e115 (2017).
224 10 Deng, Y. *et al.* Epigenetic regulation of antagonistic receptors confers rice blast resistance with
225 yield balance. *Science* **355**, 962-965 (2017).
226 11 Wang, J. *et al.* A single transcription factor promotes both yield and immunity in rice. *Science* **361**,
227 1026-1028 (2018).
228 12 Gao, M. *et al.* Ca(2+) sensor-mediated ROS scavenging suppresses rice immunity and is exploited
229 by a fungal effector. *Cell* **184**, 5391-5404.e5317 (2021).
230 13 Hu, X. H. *et al.* A natural allele of proteasome maturation factor improves rice resistance to multiple
231 pathogens. *Nat. Plants* **9**, 228-237 (2023).
232 14 Krattinger, S. G. *et al.* A putative ABC transporter confers durable resistance to multiple fungal
233 pathogens in wheat. *Science* **323**, 1360-1363 (2009).
234 15 Wang, N. *et al.* Inactivation of a wheat protein kinase gene confers broad-spectrum resistance to
235 rust fungi. *Cell* **185**, 2961-2974.e2919 (2022).
236 16 Büschges, R. *et al.* The barley *Mlo* gene: a novel control element of plant pathogen resistance. *Cell*
237 **88**, 695-705 (1997).
238 17 Li, S. *et al.* Genome-edited powdery mildew resistance in wheat without growth penalties. *Nature*

602, 455-460 (2022).

18 Lorrain, S. Lesion mimic mutants: keys for deciphering cell death and defense pathways in plants? *Trends Plant Sci.* **8**, 263-271 (2003).

19 Xing, J., Zhang, L., Duan, Z. & Lin, J. Coordination of phospholipid-based signaling and membrane trafficking in plant immunity. *Trends Plant Sci.* **26**, 407-420 (2021).

20 Liu, L., Waters, D. L., Rose, T. J., Bao, J. & King, G. J. Phospholipids in rice: significance in grain quality and health benefits: a review. *Food Chem.* **139**, 1133-1145 (2013).

21 Shimada, T. L. *et al.* Enrichment of phosphatidylinositol 4,5-bisphosphate in the extra-invasive hyphal membrane promotes colletotrichum infection of *Arabidopsis thaliana*. *Plant Cell Physiol.* **60**, 1514-1524 (2019).

22 Li, G. *et al.* The sequences of 1504 mutants in the model rice variety Kitaake facilitate rapid functional genomic studies. *Plant Cell* **29**, 1218-1231 (2017).

23 You, Q. *et al.* An E3 ubiquitin ligase-BAG protein module controls plant innate immunity and broad-spectrum disease resistance. *Cell Host Microbe* **20**, 758-769 (2016).

24 Zhao, X. *et al.* A novel glycine-rich domain protein, GRDP1, functions as a critical feedback regulator for controlling cell death and disease resistance in rice. *J. Exp. Bot.* **72**, 608-622 (2021).

25 Liu, Q. *et al.* OsCUL3a negatively regulates cell death and immunity by degrading OsNPR1 in rice. *Plant Cell* **29**, 345-359 (2017).

26 Zhou, Y. *et al.* Extraplastidial cytidinediphosphate diacylglycerol synthase activity is required for vegetative development in *Arabidopsis thaliana*. *Plant J.* **75**, 867-879 (2013).

27 Blunsom, N. J. & Cockcroft, S. CDP-diacylglycerol synthases (CDS): gateway to phosphatidylinositol and cardiolipin synthesis. *Front. Cell Dev. Biol.* **8**, 63 (2020).

28 Li, J. & Wang, X. Phospholipase D and phosphatidic acid in plant immunity. *Plant Sci.* **279**, 45-50 (2019).

29 Khang, C. H. *et al.* Translocation of *Magnaporthe oryzae* effectors into rice cells and their subsequent cell-to-cell movement. *Plant Cell* **22**, 1388-1403 (2010).

30 Du, X. Q., Yao, H. Y., Luo, P., Tang, X. C. & Xue, H. W. Cytidinediphosphate diacylglycerol synthase-mediated phosphatidic acid metabolism is crucial for early embryonic development of *Arabidopsis*. *PLoS Genet.* **18**, e1010320 (2022).

31 Hong, Y., Yuan, S., Sun, L., Wang, X. & Hong, Y. Cytidinediphosphate-diacylglycerol synthase 5 is required for phospholipid homeostasis and is negatively involved in hyperosmotic stress tolerance. *Plant J.* **94**, 1038-1050 (2018).

32 Di Paolo, G. & De Camilli, P. Phosphoinositides in cell regulation and membrane dynamics. *Nature* **443**, 651-657 (2006).

33 Kale, S. D. *et al.* External lipid PI3P mediates entry of eukaryotic pathogen effectors into plant and animal host cells. *Cell* **142**, 284-295 (2010).

34 Liu, L. *et al.* The *Xanthomonas* type III effector XopAP prevents stomatal closure by interfering with vacuolar acidification. *J Integr Plant Biol* **64**, 1994-2008 (2022).

35 Wang, H. *et al.* A plant virus hijacks phosphatidylinositol-3,5-bisphosphate to escape autophagic degradation in its insect vector. *Autophagy* **19**, 1128-1143 (2023).

36 Marković, V. & Jaillais, Y. Phosphatidylinositol 4-phosphate: a key determinant of plasma membrane identity and function in plants. *New Phytol.* **235**, 867-874 (2022).

37 Boni, R. *et al.* Pathogen-inducible *Ta-Lr34res* expression in heterologous barley confers disease resistance without negative pleiotropic effects. *Plant Biotechnol. J.* **16**, 245-253 (2018).

38 Gruner, K. *et al.* Evidence for allele-specific levels of enhanced susceptibility of wheat *mlo* mutants to the hemibiotrophic fungal pathogen *Magnaporthe oryzae* pv. *Triticum*. *Genes (Basel)* **11** (2020).

39 Li, W., Deng, Y., Ning, Y., He, Z. & Wang, G. L. Exploiting broad-spectrum disease resistance in crops: from molecular dissection to breeding. *Annu Rev Plant Biol* **71**, 575-603 (2020).

40 Oliva, R. *et al.* Broad-spectrum resistance to bacterial blight in rice using genome editing. *Nat. Biotechnol.* **37**, 1344-1350 (2019).

41 Lu, Y. *et al.* Targeted, efficient sequence insertion and replacement in rice. *Nat. Biotechnol.* **38**, 1402-1407 (2020).

Figure legends

Fig.1 | Cloning of the *RBL1* gene from the lesion mimic mutant *rbl1*, which has enhanced immunity.

a, *rbl1* mutant and wild-type (WT, KitaakeX) plants at 40 days post sowing (dps). Bar, 10 cm. **b**, Spontaneous lesions. Bar, 1 cm, which is the same for other panels without specifications. **c**, Inoculation of rice lines with *Xoo* at 14 days post-inoculation (dpi) and lesion length (**d**). **e**, Punch inoculation with *M. oryzae* at 14 dpi. The dashed lines indicate the leaf area covered by aluminum foil before spontaneous lesions appeared. **f**, Lesion area and relative fungal biomass. **g**, Fungal infection rates at 72 hours post-inoculation (hpi). **h**, Rice sheath cells infected by eGFP-tagged *M. oryzae* strain ZB25. Bars, 25 μm. **i**, ROS generation in rice plants challenged with chitin and water (mock). **j**, Screenshot of the 29-bp deletion in *rbl1*. **k**, Gene structure of *RBL1*. The gray box indicates the exon skipped in *rbl1*. The sequence of the deletion is shown, and the intron sequence is italic with the intron recognition site *"GT"* underlined. **l**, The predicted secondary structure of RBL1. The red box indicates the truncation. The CDS signature motif is shown at the bottom. **m**, 10-week-old WT, *rbl1*, and complemented (CoR1) plants. Bar, 10 cm. **n**, Leaves of the lines in (**m**). **o**, qRT-PCR assays of *RBL1*. **p**, Infected leaves, lesion area and relative fungal biomass of rice lines with *M. oryzae* at 14 dpi. Data are displayed as box and

whisker plots with individual data points: center line, median; box limits, 25th and 75th percentiles. Asterisks indicate significant differences using the unpaired Student's *t*-test (**P < 0.01, ***P < 0.001, ****P < 0.0001). Significant differences indicated by different letters in (**o**) and (**p**) were calculated using the Duncan's new multiple range test.

Fig.2 | RBL1 functions as a CDP-DAG synthase.

a, *RBL1* rescues the growth defect of the yeast *cds1* mutant. WT, yeast strain BY4741; cdsC, yeast mutant *cds1* expressing *RBL1.* **b**, Immunoblotting analysis of the RBL1-6×His fusion protein (monomeric and dimeric states). CBB, Coomassie brilliant blue. **c**, Lipidomics assays of yeast strains cultured in YPGal or YPD. **d**, Lipidomic analysis of the 4-week-old wild-type (WT, Kitaake) and *rbl1* lines. DW, dry weight. **e**, Fatty acid species of PI. No alterations were detected between WT and *rbl1* for fatty acid species 36:1 to 36:6. **f**, 8-week-old T1 plants of the *OsPIS1* overexpression OPIS1::*rbl1* lines. Bar, 10 cm. **g**, Lesions on new rice leaves. Bar, 1 cm. **h**, Lesion area of the lines in (**g**). **i**, qRT-PCR assays of genes in the OPIS1::*rbl1* line. **j**, Punch inoculation with *M. oryzae* and relative fungal biomass at 14 dpi. Bar, 1 cm. **k**, PI, PIP, and PIP_2 assays. **l**, 8-week-old plants. OPAH2::*rbl1*, the *rbl1* line overexpressing *OsPAH2*. Black bar, 1 cm; white bar, 10 cm. **m**, qRT-PCR assays. **n**, Punch inoculation with *M. oryzae* and the lesion area at 14 dpi. Bar, 1 cm. **o**, Lipidomics assays of different rice lines. The box plot elements are: center line, median; box limits, 25th and 75th percentiles. Bars in (**c**), (**h**), (**i**), and (**k**) indicate standard deviations, and asterisks in (**d**), (**e**), (**h**), and (**i**) indicate significant differences using the unpaired Student's *t*-test (*P < 0.05, **P < 0.01, ***P < 0.001, ****P < 0.0001). Significant differences indicated by different letters in (**c**), (**i**), (**j**), (**k**), (**m**), (**n**), and (**o**) were calculated using the Duncan's new multiple range test.

Fig. 3 | PI(4,5)P_2, enriched in infection-specific structures, is reduced in *rbl1* plants.

a, Dot blotting of membrane PIP_2 in the wild-type (WT, Kitaake) and *rbl1* lines. **b**, The relative levels of membrane PIP_2. **c**, Epidermal cells of rice lines expressing the PI(4,5)P_2 biosensor. Bar, 25 μm. **d**, Relative fluorescence intensity of the PI(4,5)P_2 biosensor in (**c**). The box plot elements are: center line, median; box limits, 25th and 75th percentiles. **e**, Immunoblotting of the PI(4,5)P_2 biosensor in (**c**). PLC, the biosensor; RBC, ribulose-1,5-bis-phosphate carboxylase/oxygenase. **f**, PI(4,5)P_2 aggregates around the infectious hyphal tip of *M. oryzae* at 22 hpi. AP, appressorium; IH, invasive hyphae. Pwl2 is a cytoplasmic effector, a biomarker for the biotrophic interfacial complex (BIC). Bar, 10 μm. **g**, Rice cells of the WT expressing the PI(4,5)P_2 biosensor infected by the *M. oryzae* strain expressing the apoplastic effector Bas4 tagged with the mCherry protein at 27 hpi. EIHM, extra-invasive hyphal membrane. Bar, 10 μm. **h**, Fluorescence intensity of the plasma membrane (PM) and EIHM shown in (**g**). **i**, PI(4,5)P_2 and Pwl2 at the BIC at 32 hpi. The inset shows the enlarged BIC. Bars, 5 μm. **j**, BIC formation in different rice lines. Bar, 10 μm. The numbers represent the BIC formation rates from 150 infected cells. **k**,

Working model of RBL1 in rice resistance to *M. oryzae*. RBL1 is important for the biosynthesis of PI and PIPs including $PI(4,5)P_2$. As *M. oryzae* invades, $PI(4,5)P_2$ is recruited to the EIHM and enriched in BIC. Accumulation of PA is a minor factor of enhanced immunity of *rbl1*. Other unknown factors also contribute to enhanced immunity of *rbl1*. Bars in (**b**) and (**h**) indicate standard deviations, and asterisks indicate significant differences using the unpaired Student's *t*-test (****$P < 0.0001$).

Fig.4 | *RBL12* confers broad-spectrum resistance with no observed yield penalty in field trials. **a**, Guide RNA sites, indicated by dots, for genome editing of *RBL1*. The asterisk indicates the edited site in *RBL12*. **b**, *RBL1* edited lines. WT, Kitaake. Bar, 1 cm, which is the same for other panels without specifications. **c**, 8-week-old plants in the greenhouse. Bar, 10 cm. **d**, Agronomic traits. **e**, Lesions with *M. oryzae* at 14 dpi. **f**, Lesions with *Xoo* at 14 dpi. **g**, *In planta* bacterial growth of *Xoo* strain PXO99. **h**, Infected panicles with *U. virens*. Rice false smut balls were counted at 17 dpi. **i**, Quantitative assays of ustiloxins in infected panicles. FW, fresh weight. **j**, Infected spikelets with *U. virens*. Arrows indicate invasive hyphae. an, anther; pa, palea; sf, stamen filament; st, stigma. Bars, 100 μm. **k**, Rice grain yield in the "Normal" field trials with low incidence of rice blast. **l**, Field assessment of blast resistance in the blast nursery. Representative panicles are shown on the left. Disease severity is indicated by the percentage of necrotic panicles for each plant caused by *M. oryzae*. **m**, Grain yield of plants grown in the blast nursery. Seeds per plant are shown on the left. The box plot elements are: center line, median; box limits, 25th and 75th percentiles. Asterisks in (**h**), (**i**), (**l**), and (**m**) indicate significant differences using the unpaired Student's *t*-test (*$P < 0.05$, ***$P < 0.001$, ****$P < 0.0001$). Significant differences indicated by different letters in (**d-g**) were calculated using the Duncan's new multiple range test.

Online content

Any methods, additional references, Nature Research reporting summaries, source data, supplementary information, acknowledgements, peer review information; details of author contributions and competing interests; and statements of data and code availability are available at https://doi.org/.

Methods

Plant materials, strains, and growth conditions

The *rbl1* mutant (FN398) was identified from the FN-induced mutant population generated in the model *Japonica* rice (*Oryza sativa*) line KitaakeX[42]. The genome sequence of KitaakeX is available online (https://phytozome.jgi.doe.gov/pz/portal.html)[43]. The segregating M3 population derived from the *rbl1* line was used in sequencing and cosegregation assays. For infection assays and other phenotype characterizations, rice seeds were surface-sterilized and germinated on 1/2 Murashige and Skoog (MS) media. After a week in the growth chamber, plants were transferred to the greenhouse with a photoperiod (12/12 h) at 28°C. The Arabidopsis plants were cultivated in the potting soil mixture (peat soil/rich soil/vermiculite =1:1:1, v/v/v) in growth chamber at 21°C, 60% humidity, the day/night period

16/8 h, with an intensity of 80 μmol m^{-2} s^{-1} (ref.[30,44]). The *Xanthomonas oryzae* pv. *oryzae* (*Xoo*) strain was grown on nb plates at 28°C for 3 days before use[45]. The *Magnaporthe oryzae* strains were cultured on oatmeal agar plates under light at room temperature[46,47]. The *Ustilaginoidea virens* strains were routinely grown on PSA plates and were grown in the PSB medium at 28°C, 160 rpm for 7 days for conidiation[48]. The *Phytophthora capsica* strain was cultured on PDA plates at 25°C for 3-4 days in dark before use[49].

Generation of *M. oryzae* strains tagged with different fluorescence proteins

Fungal protoplast preparation and transformation were performed as previously described[50]. Briefly, the GFP overexpression plasmid RP27-GFP, the apoplastic effector Bas4-mCherry vector that was used to indicate the extra-invasive hyphal membrane (EIHM), and the cytoplasmic effector Pwl2-mCherry vector that was used to indicate the biotrophic interfacial complex (BIC), were transformed into *M. oryzae* strain ZB25 (ref.[29,51]). The resultant transformants were selected on TB3 plates with 500 μg/ml geneticin (GLPBIO). The neomycin-resistant transformants were verified using PCR and examined under a laser scanning confocal microscopy.

Plant infection assays

The leaf-clipping method was used in *Xoo* infection of rice plants at the booting stage[52]. The *Xoo* culture of strains PXO71, PXO99, PXO341, ZHE173 and GX01 (ref.[53]) was suspended in distilled water and the bacterial suspension concentration was adjusted to OD600 ≈ 0.5. A pair of sterilized scissors were dipped into the bacterial suspension and cut the leaves at 5 cm from the leaf tip. The infected plants were transferred to the greenhouse. The setting for the greenhouse was the day/night period (12/12 h), temperature (~28°C), and relative humidity (80%). Water-soaked lesions were scored at 14 days post-inoculation (dpi) or as indicated. At least three plants were inoculated for each assay. The *ΔraxST Xoo* strain that can overcome the XA21-mediated immunity was used to infect the KitaakeX line carrying the *Xa21* gene[53].

The *M. oryzae* strains ZB25, LN3, LN13, LN14, ES18, ES24, ES28, ES36, ES76, and ES80 used in infection assays were isolated from the rice fields in Enshi (ES) and Liaoning (LN), China and stored in the laboratory. The punch inoculation was conducted as previously described[54]. Briefly, spores were freshly collected from 10-day-old oatmeal agar cultures and the concentration was adjusted to 1×10^5 spores/ml with 0.025% Tween-20. Fully extended rice leaves at 30 days post-sowing (dps) were wounded with a punch and inoculated with 10 μl spore suspension. The punched area was sealed with clear Scotch tapes. Inoculated plants were transferred to the greenhouse. Symptoms were scored at 14 dpi and relative fungal biomass abundance was measured using the qPCR approach[25]. Primers used in the assay are listed in Supplementary Table 1.

For microscopic analysis of *M. oryzae* infection, the ZB25-eGFP strain stably expressing the GFP was used to inoculate detached rice sheaths of 5-week-old rice plants. The spore concentration was adjusted to approximately 1.5×10^6 conidia/ml. The fungal infection rate in each plant line was analyzed from five replicates at 72 hpi, and at least 30 appressoria for each replicate were examined for invasive hyphae growth in the rice sheath cells under a laser scanning confocal microscopy (Leica TCS SP8).

For false smut infection with *U. virens* strains HWD2 and JS60 (ref.[55]), panicles of rice plants at the booting stage were inoculated with 1 ml of a mixture of spores and homogenized mycelia with a syringe. Infected plants were kept at ~25°C with ~85% relative humidity in the greenhouse. The number of smut balls per panicle was counted at 17 dpi. For scanning electron microscope (SEM), spikelet was sampled from the Kitaake and *RBL12* lines inoculated at 36 h, 72 h, and 7 d, and directly examined with SEM (JSM-6390/LV) using the protocol previously described[56].

Infection assays on Arabidopsis with *Phytophthora capsica* were conducted as previously described with minor modifications[49]. Briefly, the *P. capsici* strain LT263 was cultured on PDA plates for 3 days at 25°C in dark. Detached leaves of Arabidopsis at 30 dps were placed on the 0.8% water-agar plates and inoculated with 3 mm x 3 mm blocks of the *P. capsica* culture. The samples were kept at room temperature in darkness. The inoculated leaves were photographed under UV light, and the lesion area and relative pathogen biomass were measured at 36 hpi.

DAB staining

To visualize hydrogen peroxide (H_2O_2) in the plant tissue, rice leaves were collected at 40 dps and immediately immersed in the 3, 3'-diaminobenzidine (DAB) staining solution (1 mg/ml) in 15 ml tubes. The tube was covered with aluminum foil and incubated with shaking at 80-100 rpm at room temperature for 8 h. Samples were decolored with 95% ethanol in a boiling water bath for 10 min and bleached for another 48 h in fresh 95% ethanol until the chlorophyll had been mostly removed from the sample. The cleared leaves were then visualized for DAB staining.

Measurement of reactive oxygen species

Measurement of ROS following chitin treatment was conducted as previously described[25]. Briefly, rice plants were grown on 1/2 MS media in the growth chamber for 12 days. Leaves of the seedlings were cut into disks (3 mm×3 mm) and then submerged in distilled water in a 96-well plate under light overnight. The distilled water was pipetted out and replaced with 100 µl mixed solution for each well, which contains 50 µM luminol (Wako), 10 µg/ml horseradish peroxidase and 8 nM chitin (GLPBIO), using a multiple-channel pipette. The chemiluminescence was measured at 500-ms intervals over a period of 40 min in a SPARK-10M microplate reader (TECAN). Three biological replicates, each of which contains eight technical replicates, were used for each sample. Distilled water was used as the mock control.

Quantitation of total salicylic acid in leaf

For total salicylic acid (SA) measurement, plants were grown on 1/2 MS media in the growth chamber for 12 days, and leaf tissues were harvested and freeze dried. About 20 mg dried tissues were ground in liquid nitrogen. The sample powder was mixed with 1 ml 80% (v/v) methanol using an ultrasonic cleaner at 70°C for 15 min. The mixture was centrifuged at 7,000×g at 4°C, and the supernatant was collected and filtered (Φ 0.22 μm). SA in the samples and serial dilutions of the SA standard were analyzed together using the high-performance liquid chromatography-tandem mass spectrometry (HPLC-MS) system. The SA content of each sample was calculated by comparing with the calibration curve of the SA standard.

RNA extraction, and reverse-transcription quantitative PCR analysis

Rice leaves as indicated were sampled into liquid nitrogen. RNA was isolated with TRIzon (CWBIO). Residual DNA was eliminated with DNase I (Thermo Scientific). Purified RNA was examined using agarose gel electrophoresis before complementary DNA (cDNA) synthesis, which was performed using the HiScript II 1st Strand cDNA Synthesis Kit (Vazyme). qRT-PCR was performed on a Bio-Rad CFX96 Real-Time System coupled to a C1000 Thermal Cycler (Bio-Rad) using the SYBR Green Mix (Vazyme). The $2^{-\Delta\Delta CT}$ method was used to calculate the expression level of target genes[57]. Three biological replicates for each of which included three technical replicates were used for each sample. The rice *Actin* gene (LOC_Os03g50885, NM_001058705) was used as the internal control. See Supplementary Table 1 for primers used.

Cloning of *RBL1* and genetic complementation

The *rbl1* mutant was crossed with Kitaake and the F1 plants were used to examine whether the spontaneous lesion phenotype was controlled in a recessive/dominant manner. DNA was isolated from pooled samples of three M3 plants showing spontaneous lesions of the *rbl1* line. Genomic sequencing performed on the HiSeq 2500 next-generation sequencing system (Illumina) and mutation identification using the established bioinformatic pipeline were conducted as described[22]. InDel markers for identified homozygous mutations were used in the cosegregation assay (Supplementary Table 1). Primers RBL1cDNAF/R were used to amplify the coding sequence of *RBL1* from cDNA of Kitaake and the *rbl1* mutant and the resultant products were sequenced. To complement the *rbl1* mutant, the entire ORF of the *RBL1* gene including its native promoter, 2-kb sequence upstream of the start codon ATG, was amplified using PCR with primers CoRBL1F/R (Supplementary Table 1). The PCR product was purified and then cloned into the binary vector pCAMBIA2300 using a HiFi DNA Assembly Master Mix (NEB). The resultant construct was confirmed using Sanger sequencing. The following *Agrobacterium*-mediated transformation and transformant selection were performed at BioRun BioScience Co., Ltd. (Wuhan, China). The positive transformants were examined using the Cleaved Amplified Polymorphic Sequences

(CAPS) marker (Supplementary Table 1). *RBL1* expression and fungal infection assays were done as described above.

Yeast mutant complementation and protein purification

The *RBL1* ORF was amplified from Kitaake cDNA with primers YCF1/R1 (Supplementary Table 1) and cloned into plasmid pYES2-His as pYES2-*RBL1*-His. Competent cells of the yeast strain BY4741 (*MATa his3 leu2 met15 ura3*) (WT) were prepared and transformed with the pYES2-*RBL1*-His construct using the Super Yeast Transformation Kit (Coolaber). The Ura^+ transformant was confirmed using PCR and then used in knocking out the yeast endogenous *CDS1* gene using a homologous recombination approach[58]. The resultant strains were confirmed using PCR and assayed for growth on YPD and YPGal plates at 30°C. To analyze the RBL1 protein expression in yeast, the total protein was isolated from the complementation and WT strains, and the His-tagged RBL1 protein was detected using western blotting with anti-His-tag antibody (1:5,000 dilution; CST). Functional complementation assays with the RBL1-GFP fusion protein were performed similarly.

For protein expression and purification, total proteins were isolated from yeast strains BY4741, and transformants carrying pYES2-*RBL1*-His and pYES2-*RBL12*-His. The His-tagged RBL1 and RBL12 proteins were purified from total proteins using the Ni-NTA protein purification system according to a method described previously[2]. The thermostability assays of the fusion proteins were performed using the differential scanning calorimeter (DSC) as previously described[59]. Briefly, the temperature range was set from -100°C to 150°C, and the scan rate was 60°C/h.

Yeast lipidomics assays

To analyze functions of RBL1 in yeast, the WT and complementation yeast strains were cultured in YPGal to reach OD600 ≈ 0.6, and the yeast cells were harvested using brief centrifugation and rinsed with sterile water once. The yeast cells were then resuspended in YPD or YPGal and cultured at 30°C, 220 rpm for up to 4, 8, and 20 h before harvesting for phospholipid isolation. The yeast cells were then homogenized with acid-washed glass beads, and 1 ml extraction buffer chloroform/methanol/formic acid (10:10:1, v/v/v) was added to the homogenized yeast cells and vortexed for 3 min and centrifuged at 4°C, 1,000×g for 6 min to collect the supernatant. The extraction was repeated once with chloroform/methanol/water (5:5:1, v/v/v). The supernatant was combined and mixed well with 3 ml buffer (0.2 M H_3PO_4, 1 M KCl). The mixture was centrifuged at 4°C, 1,000×g for 10 min. The lower organic phase was collected and dried under the nitrogen gas. The dried sample was dissolved in 300 µl chloroform, and lipid extracts were analyzed using liquid chromatography-mass spectrometry (LC-MS/MS) as previously described[60].

Protein subcellular localization analysis

The full-length coding sequence of *RBL1* was amplified with primers SLRBL1F/R (Supplementary Table 1) and fused with the enhanced green fluorescent protein (eGFP) sequence in vector pEarleyGate101 under control of the CaMV 35S promoter[44]. The resultant constructs were confirmed using Sanger sequencing and transformed into *Nicotiana benthamiana* leaves with/without related marker constructs. For *N. benthamiana* transient expression, constructs were transformed into *Agrobacterium* strain GV3101 and then the resultant strain was infiltrated into leaves of 30-day-old *N. benthamiana* plants. The fluorescence signal was observed with laser scanning confocal microscopy (Leica TCS SP8) 72 h after infiltration.

GUS histochemical assay

For the β-glucuronidase (GUS) activity assay, the 2-kb genomic region upstream of the start codon of *RBL1* was PCR amplified from rice genomic DNA with primers ProRBL1-F/R (Supplementary Table 1) and cloned into the pGreenII 0179-GUS vector[44]. The resultant construct pRBL1-GUS was confirmed using Sanger sequencing and transformed into rice calli using the *Agrobacterium*-mediated approach. Plants containing pRBL1-GUS were genotyped before GUS staining. For GUS staining, rice plant tissues were stained in the Ready-to-use GUS Staining Solution (PHYGENE) at 37°C overnight. The stained plant tissues were rinsed with water and incubated in 70% ethanol for 24 h to remove the chlorophyll. Photomicrographs were taken using the stereoscopic microscope (Nikon SMZ1000).

Lipid extraction and analysis

Leaf samples from 5-week-old plants were used for the total phospholipid extraction as described[31]. Briefly, more than 10 mg fresh weight (FW) rice leaf tissue was harvested and immediately immersed in preheated isopropanol (75°C) with 0.01% butylated hydroxytoluene (BHT) and incubated for 15 min. After cooling to room temperature, chloroform was added to the sample and incubated with shaking at room temperature for 1 h. The lipid extracts were transferred to new glass tubes to repeat the extraction procedure until the leaf sample became bleached. The lipid extracts were combined and evaporated under the nitrogen gas, and then redissolved in chloroform. The lipidomics analysis was performed by a method described by Lu et al.[61] using a TripleTOF mass spectrometer (TripleTOF-MS/MS) instrument with an electrospray ionization (ESI) source in the positive ion mode. Lipids in each class were quantified by comparison with internal standards (Avanti).

Phosphoinositides were extracted as previously described[62]. Briefly, lipids from dried leaf samples of the Kitaake, *rbl1*, *RBL12*, and OPIS1 lines were extracted with 750 µl of MeOH/$CHCl_3$/1M HCl (2:1:0.1, v/v/v) and 150 µl of H_2O in the presence of internal standards. Lipids were modified with TMS-diazomethane for 10 min. LC-MS/MS (multiple-reaction-monitoring mode) analyses were performed with a mass spectrometer QTRAP 6500 (ABSciex) mass spectrometer coupled with a liquid chromatography system (1290 UPLC Infinity II, Agilent). Analyses were achieved in the positive ion mode. Reverse-phase

separations were carried out on a Jupiter C4 column (50×1 mm; particle size, 5 μm; Phenomenex). Eluent A was H_2O and 0.1% formic acid, and eluent B was acetonitrile and 0.1% formic acid. The gradient elution program was as follows: 0-2 min, 45% eluent B; 27 min, 100% eluent B; and 27-30 min, 100% eluent B. The flow rate was 100 μl/min; 10 μl sample volumes were injected. The area of LC peaks was determined using MultiQuant software (ABSciex) for relative quantification to the area of the internal standard, and values are expressed in arbitrary unit by quantity (AU/mg DW).

Chemical supplementation and overexpression of the *OsPIS1* and *OsPAH2* genes

Phospholipids PI, PG, PI(4,5)P_2, and diphenyleneiodonium chloride (DPI) were added to DMSO, and incubated at 42°C for 30 min and treated in the ultrasonic homogenizer for 10 min to facilitate the dissolving. The mixture was filter-sterilized (Φ 0.22 μm). For chemical supplementation assays, Kitaake and *rbl1* plants were grown on 1/2 MS media with PI (0, 10, 50, and 100 μM), PG (0, 10, and 100 μM), PI(4,5)P_2 (0, 50, and 100 nM), PA (0, 0.1, 1, and 10 μM), or DPI (0, 0.1, 0.5, and 1 μM) in the growth chamber for 6~10 days. The leaf was then examined for lesions for a successive of 10 days. To overexpress *OsPIS1* and *OsPAH2* genes, genomic regions of these two genes were cloned into vector pRGV under control of the maize *Ubiquitin10* promoter[63], respectively. The resultant constructs were sequenced and transformed into the *rbl1* mutant. The overexpression lines were genotyped, analyzed using qRT-PCR and examined for lesions. Plant infection assays and related qRT-PCR assays of the overexpression line were performed as described above.

Plasma membrane extraction and lipid blotting assay

The plasma membrane enrichment and purification were performed using aqueous two-phase partitioning as described previously[64]. Briefly, rice leaves (20 g) were homogenized in liquid nitrogen, and were immediately added to 120 ml ice-cold buffer (50 mM Tris-Me (pH 8.0), 0.25 M sucrose, 3 mM EDTA, 0.6% PVP, 10% glycerol, 10 mM DTT, 1 mM PMSF, 1×protease inhibitor cocktail). When the homogenized tissues were obtained, one small portion of the sample was used to extract proteins for the loading control; the remaining sample was used to extract membrane lipids. The samples were centrifuged at 60,000×g for 30 min to pellet plasma membrane vesicles. The plasma membrane was then mixed with 1 ml of chloroform/methanol/concentrated HCl (1:2:0.02, v/v/v) solution, and the lipid components were separated using 300 μl of chloroform and 300 μl of KCl (2 M).

In the subsequent lipid dot blotting, the organic phase was applied to the nitrocellulose filter membrane, and PIP_2 was detected with the mouse anti-PIP_2 antibody 2C11 (Abcam), which were conducted following a previously described method[65]. ImageJ software was used to quantify the content of PIP_2 on the blotted membrane.

Subcellular localization and fluorescence intensity assays of rice PIP and PIP_2

A set of vectors genetically encoding biosensors for PIP and PIP_2 were ordered from the Nottingham Arabidopsis Stock Centre, including mCIT-2×$FYVE^{HRS}$ for PI3P, mCIT-2×PH^{FAPP1} for PI4P, and mCIT-1×$PH^{PLC\Delta1}$ for $PI(4,5)P_2$ (ref.[66]). To analyze the subcellular localization of PIP in rice protoplasts, we cloned the 1×$FYVE^{HRS}$, 1×PH^{FAPP1}, and 1×$PH^{PLC\Delta1}$ fragments into the pM999-eGFP vector under control of the CaMV 35S promoter. The resultant constructs were confirmed using Sanger sequencing and transformed into rice protoplasts. Rice protoplast preparation and transformation were performed as described[67]. Fluorescence intensity of PIP was quantified using ImageJ based on the methods described previously[62]. The ratio of the total fluorescence signals to the signals at the plasma membrane was calculated.

To generate rice lines stably expressing genetically encoded biosensors for $PI(4,5)P_2$, we cloned the 1x$PH^{PLC\Delta1}$ fragment into the pRGV-eGFP vector under control of the maize *Ubiquitin10* promoter[63]. The resultant vector was verified by sequencing and transformed into Kitaake and *RBL12*, which was further crossed with *rbl1*. Confocal laser scanning microscopy was performed using the laser scanning confocal microscopy (Leica TCS SP8). Intactness of the $PI(4,5)P_2$ biosensor in rice was examined using western blotting as described[68]. Briefly, rice leaf tissues were ground to fine powder with a mortar and pestle in liquid nitrogen and solubilized in the extraction buffer (50 mM Tris-HCl pH 7.5; 150 mM NaCl; 1 mM EDTA; 1% Tritonx-100; 0.5 mM PMSF; 1% protease inhibitor cocktail). The protein extracts were centrifuged at 12,000×g at 4°C, and the supernatant was cleared through a filter (Φ 0.45 μm). We mixed 70 μl protein exacts, 10 μl 0.4 M DTT, 20 μl 5×SDS loading buffer and 1 μl β-mercaptoethanol and took 20 μl mixed sample to run 10% SDS-PAGE. The blotting was performed on the PVDF membrane (Bio-Rad). The primary antibody was anti-GFP (1:1,000, Cell Signaling Technology) and western blotting was following the manufacturer's instructions. Coomassie brilliant blue (CBB) staining of rice ribulose bisphosphate carboxylase/oxygenase (Rubisco) was used as the internal control[69].

To analyze the subcellular localization of rice $PI(4,5)P_2$ during *M. oryzae* infection, the verified T2 plants were used to observe subcellular locations of $PI(4,5)P_2$ in rice sheath cells[70], inoculated with the *M. oryzae* ZB25 strains expressing Pwl2-mCherry or Bas4-mCherry. The fluorescence signal was detected using the confocal microscope Nikon N-STORM with the following settings of excitation/emission wavelengths: GFP (488/505 to 530 nm) and mCherry (561/587 to 610 nm).

Genome editing

Genome editing of *RBL1* was conducted using a previously described method[71]. Briefly, guide RNAs (gRNAs) for genome editing were selected assisted by an online program CRISPR-Plant[72]. Related primers were designed (Supplementary Table 1) and the gRNA cassette was assembled into vector pBER32 as described[71]. After being confirmed using Sanger sequencing, the binary constructs were transformed into embryogenic calli of Kitaake, Nipponbare, and Zhonghua11 using *Agrobacterium*-

mediated transformation. The resultant transformants were genotyped using Sanger sequencing, and the sequence was analyzed using DSDecodeM[73]. The confirmed edited lines were analyzed for plant growth, *RBL* expression, and plant immunity phenotypes.

Field trials of the edited lines

Field yield and resistance to blast were assessed at the experimental stations (Hainan, Hubei, and Jiangxi) with “normal field” (low incidence of rice blast) and blast nursery (high incidence of rice blast) in the summer season, respectively. Enshi (Hubei) was selected because this mountainous area has a high incidence of rice blast disease each year[10]. Design of the field plots was conducted following the strategy established by the International Rice Research Institute (IRRI)[74]. For each field trial, plants were grown with either 10 (Hainan) or 5 (Hubei and Jiangxi) replicate plots for each line, and each plot contained 100 plants that were 20 cm apart. Diseased plantlets of the blast susceptible line Lijiangxintuanheigu (LTH) were used as a source of inoculum for spreading the disease[73]. One row of LTH was sown for every 10 rows of test accessions, and disease was allowed to spread naturally via wind dispersal. In the “normal field”, we did not include spreader row. Rice blast resistance of different lines was evaluated according to the IRRI evaluation system, and the percentage of necrotic panicles due to blast was calculated[74].

Data availability

Sequencing data for the pooled M3 plants derived from the *rbl1* line (FN398) are available at the National Center for Biotechnology Information under the accession number of SRR4096918. Other sequences can be accessed under the following numbers: *RBL1* (LOC_Os01g55360, NP_001044302.1), *OsPIS1* (LOC_Os02g03110, NC_029257.1) and *OsPAH2* (LOC_Os11g40080, XP_015617116.1).

References

42 Li, G. *et al.* Genome-wide sequencing of 41 rice (*Oryza sativa* L.) mutated lines reveals diverse mutations induced by fast-neutron irradiation. *Mol Plant* **9**, 1078-1081 (2016).

43 Jain, R. *et al.* Genome sequence of the model rice variety KitaakeX. *BMC Genom.* **20**, 905 (2019).

44 Tang, J. *et al.* GDSL lipase occluded stomatal pore 1 is required for wax biosynthesis and stomatal cuticular ledge formation. *New Phytol.* **228**, 1880-1896 (2020).

45 Park, C. J. & Ronald, P. C. Cleavage and nuclear localization of the rice XA21 immune receptor. *Nat. Commun.* **3**, 920 (2012).

46 Zhou, X. *et al.* Loss of function of a rice TPR-domain RNA-binding protein confers broad-spectrum disease resistance. *Proc. Natl. Acad. Sci. USA* **115**, 3174-3179 (2018).

47 Li, G. *et al. MST50* is involved in multiple MAP kinase signaling pathways in *Magnaporthe oryzae*. *Environ. Microbiol.* **19**, 1959-1974 (2017).

48 Li, G. B. *et al.* Overproduction of OsRACK1A, an effector-targeted scaffold protein promoting

644 OsRBOHB-mediated ROS production, confers rice floral resistance to false smut disease without yield
645 penalty. *Mol Plant* **15**, 1790-1806 (2022).
646 49 Li, Q. *et al.* A *Phytophthora capsici* effector targets ACD11 binding partners that regulate ROS-
647 mediated defense response in *Arabidopsis*. *Mol Plant* **12**, 565-581 (2019).
648 50 DeZwaan, T. M., Carroll, A. M., Valent, B. & Sweigard, J. A. *Magnaporthe grisea* Pth11p is a novel
649 plasma membrane protein that mediates appressorium differentiation in response to inductive substrate
650 cues. *Plant Cell* **11**, 2013-2030 (1999).
651 51 Jones, K. *et al.* Disruption of the interfacial membrane leads to *Magnaporthe oryzae* effector re-
652 location and lifestyle switch during rice blast disease. *Front. Cell Dev. Biol.* **9**, 681734 (2021).
653 52 Chen, X. *et al.* An ATPase promotes autophosphorylation of the pattern recognition receptor XA21
654 and inhibits XA21-mediated immunity. *Proc. Natl. Acad. Sci. USA* **107**, 8029-8034 (2010).
655 53 Luu, D. D. *et al.* Biosynthesis and secretion of the microbial sulfated peptide RaxX and binding to
656 the rice XA21 immune receptor. *Proc. Natl. Acad. Sci. USA* **116**, 8525-8534 (2019).
657 54 Fan, J. *et al.* The monocot-specific receptor-like kinase SDS2 controls cell death and immunity in
658 rice. *Cell Host Microbe* **23**, 498-510.e495 (2018).
659 55 Chen, X. *et al.* The 'pears and lemons' protein UvPal1 regulates development and virulence of
660 *Ustilaginoidea virens*. *Environ. Microbiol.* **22**, 5414-5432 (2020).
661 56 Fan, J. *et al.* The false smut pathogen *Ustilaginoidea virens* requires rice stamens for false smut
662 ball formation. *Environ. Microbiol.* **22**, 646-659 (2020).
663 57 Livak, K. J. & Schmittgen, T. D. Analysis of relative gene expression data using real-time
664 quantitative PCR and the $2^{-\Delta\Delta CT}$ method. *Methods* **25**, 402-408 (2001).
665 58 Haselier, A., Akbari, H., Weth, A., Baumgartner, W. & Frentzen, M. Two closely related genes of
666 Arabidopsis encode plastidial cytidinediphosphate diacylglycerol synthases essential for
667 photoautotrophic growth. *Plant Physiol.* **153**, 1372-1384 (2010).
668 59 Durowoju, I. B., Bhandal, K. S., Hu, J., Carpick, B. & Kirkitadze, M. Differential scanning
669 calorimetry - a method for assessing the thermal stability and conformation of protein antigen. *J Vis Exp*
670 (2017).
671 60 Li, Q. *et al.* Understanding the biochemical basis of temperature-induced lipid pathway adjustments
672 in plants. *Plant Cell* **27**, 86-103 (2015).
673 61 Lu, S., Liu, H., Jin, C., Li, Q. & Guo, L. An efficient and comprehensive plant glycerolipids analysis
674 approach based on high-performance liquid chromatography-quadrupole time-of-flight mass
675 spectrometer. *Plant Direct* **3**, e00183 (2019).
676 62 Ito, Y. *et al.* Sphingolipids mediate polar sorting of PIN2 through phosphoinositide consumption at
677 the trans-Golgi network. *Nat. Commun.* **12**, 4267 (2021).

63 He, F., Zhang, F., Sun, W., Ning, Y. & Wang, G. L. A versatile vector toolkit for functional analysis of rice genes. *Rice (N Y)* **11**, 27 (2018).

64 Santoni, V. Plant plasma membrane protein extraction and solubilization for proteomic analysis. *Methods Mol. Biol.* **355**, 93-109 (2007).

65 Yang, H. *et al.* Pore architecture of TRIC channels and insights into their gating mechanism. *Nature* **538**, 537-541 (2016).

66 Colin, L. *et al.* Imaging the living plant cell: From probes to quantification. *Plant Cell* **34**, 247-272 (2022).

67 Tang, N. *et al.* MODD mediates deactivation and degradation of OsbZIP46 to negatively regulate ABA signaling and drought resistance in rice. *Plant Cell* **28**, 2161-2177 (2016).

68 Zhai, K. *et al.* NLRs guard metabolism to coordinate pattern- and effector-triggered immunity. *Nature* **601**, 245-251 (2022).

69 Gutteridge, S. & Gatenby, A. A. Rubisco synthesis, assembly, mechanism, and regulation. *Plant Cell* **7**, 809-819 (1995).

70 Simon, M. L. *et al.* A multi-colour/multi-affinity marker set to visualize phosphoinositide dynamics in Arabidopsis. *Plant J.* **77**, 322-337 (2014).

71 Xie, K., Minkenberg, B. & Yang, Y. Boosting CRISPR/Cas9 multiplex editing capability with the endogenous tRNA-processing system. *Proc. Natl. Acad. Sci. USA* **112**, 3570-3575 (2015).

72 Minkenberg, B., Zhang, J., Xie, K. & Yang, Y. CRISPR-PLANT v2: an online resource for highly specific guide RNA spacers based on improved off-target analysis. *Plant Biotechnol. J.* **17**, 5-8 (2019).

73 Xie, X. *et al.* CRISPR-GE: a convenient software toolkit for CRISPR-based genome editing. *Mol Plant* **10**, 1246-1249 (2017).

74 I.R.R.I. Standard evaluation system for rice (SES). *pp*, 17-18 (2002).

Acknowledgements

We thank G. Wang (Ohio State University) and Y. Ning (Chinese Academy of Agricultural Sciences) for pRGV and pRHV vectors, and X. Chen (Sichuan Agricultural University) for *M. oryzae* stains, and Z. Wang (Fujian Agriculture and Forestry University) for Pwl2-mCherry marker, and W. Zhao (China Agricultural University) and L. Cao (China National Rice Research Institute) for rice *spl-D* and *cul3a* mutants, respectively, and H. Xue (Shanghai Jiao Tong University) for Arabidopsis *cds* mutants, and P. Fei (Huazhong University of Science and Technology) for technical support on confocal imaging, and G. Ren (Sichuan Academy of Agricultural Sciences) for field trials. At Huazhong Agricultural University, we thank H. Hu for the pEarleyGate101 vector and HDEL-mCherry markers, D. Duanmu for the pYES2-NTA vectors, and W. Chen for total salicylic acid (SA) analysis, and C. Luo, M. Yuan, and Z. Lai for *U. virens* and *Xoo* strains and Arabidopsis lines. The phospholipid analysis was performed on the

lipidomics platform of the National Key Laboratory of Crop Genetic Improvement. Phosphoinositides measurements were performed on the Bordeaux Metabolome Facility-MetaboHUB (ANR-11-INBS-0010). Confocal laser scanning microscope data were acquired at the State Key Laboratory of Agricultural Microbiology Core Facility, and we would be grateful to Z. Hu and X. Shen for their supports for data acquisition and analysis. The computation in this paper was run on the bioinformatics computing platform of the National Key Laboratory of Crop Genetic Improvement. We thank J. Zhou (CAS Institute of Genetics and Developmental Biology), X. Chen, Z. He (CAS Center for Excellence in Molecular Plant Sciences), X. Wang (Northwest A&F University), and J.R. Xu (Purdue University) for discussion. This work was supported by National Key R&D Program of China (2022YFA1304402), Natural Science Foundation of China (32172373, 31801723), Fundamental Research Funds for the Central Universities (2662020ZKPY006) and the Open Research Fund of State Key Laboratory of Hybrid Rice (Wuhan University) (KF202202) to G.L. J.C.M. is supported by the Joint Bioenergy Institute funded by the US Department of Energy (no. DE-AC02-05CH11231). Research in the Ronald Laboratory was supported by the National Science Foundation, the National Institutes of Health (GM122968 and GM55962), and the Joint Bioenergy Institute funded by the US Department of Energy (no. DE-AC02-05CH11231).

Author contributions

G.L., G.S., P.S., and P.C.R. designed the experiments. G.S., P.S., X.K., X.H., Q.S., L.F., Y.B., J.Z., Y.L., L.Y., Y.W., Q.G., Y.Z., W.Z., J.G., R.H., X.C., W.Z., Z.Q., and Q.Z. performed the experiments. G.L., G.S., P.S., X.K., X.H., L.Y., L.Z., K.X., Q.Z., T.C., J.X., R.J., J.G., Q.L., L.G., J.C.M., L.F., Y.B., and Z.K. analyzed the data. G.L. and G.S drafted the manuscript, and G.L., G.S., P.S., L.F., L.Z., L.G., K.X., J.C.M., Q.L., Y.B., Z.K., and P.C.R. revised the manuscript. All authors read and approved the final manuscript.

Competing interests

G.L., G.S. and X.H. are inventors on a provisional patent application 202111041400.3 that covers *rbl1* and *RBL12* lines.

Reporting summary

Further information on research design is available in the Nature Research Reporting Summary linked to this article.

Additional information

Supplementary information is available for this paper at https://

Correspondence and requests for materials should be addressed to P.C.R. and G.L.

Reprints and permissions information is available at www.nature.com/reprints.

Extended data figure legends

Extended Data Fig. 1 | The plant glycerolipid metabolic pathway related to cytidinediphosphate-diacylglycerol synthase 1 (CDS1).

Rice RBL1 is homologous to yeast Cds1. CDP-DAG, cytidinediphosphate-diacylglycerol; DAG, diacylglycerol; PA, phosphatidic acid; PAH, phosphatidic acid phosphohydrolase; PC, phosphatidylcholine; PE, phosphatidylethanolamine; PG, phosphatidylglycerol; PGPS, phosphatidylglycerol phosphate synthase; PI, phosphatidylinositol; PI4K, phosphatidylinositol 4-kinases; PI4P, phosphatidylinositol 4-phosphate; PI4P5K, phosphatidylinositol 4-phosphate 5-kinase; $PI(4,5)P_2$, phosphatidylinositol-4,5-bisphosphate; PIS, phosphatidylinositol synthase; PS, phosphatidylserine; PSS, phosphatidylserine synthase.

Extended Data Fig. 2 | Expression of plant defense-related genes, yield, and genetic complementation of the *rbl1* line.

a, Panicles and seeds of the *rbl1* and WT lines. Bars, 1 cm. Grain yield of the *rbl1* and WT lines. Data are displayed as box and whisker plots with individual data points. The box plot elements are: center line, median; box limits, 25th and 75th percentiles. **b**, *In situ* detection of reactive oxygen species (ROS) in the *rbl1* mutant and wild-type (WT, KitaakeX) leaves using 3,3'-diaminobenzidine (DAB) staining. Bar, 1 cm. **c**, The total salicylic acid (SA) level is increased in the *rbl1* mutant. Total SA was isolated from leaves of 2-week-old seedlings. **d**, qRT-PCR assays of marker genes of plant immunity. Total RNA was extracted from leaves of 4-week-old plants. Gene *Actin* was used as the internal control. **e**, A 29-bp deletion cosegregates with the lesion mimic phenotype in the M3 population of line *rbl1*. PCR results of InDel markers targeting the 29-bp deletion: one short band, homozygous; one large band, wild-type alleles; two bands, heterozygous. “+” indicates lesions on the leaf of the M3 plant and “-” no lesion. A $\chi 2$ test of the phenotypic ratio revealed that the actual value 26: 92 of lesioned plants to normal plants is statistically similar to the expected value 1: 3 ($\chi 2 = 0.213$, P-value = 0.644 > 0.05). **f**, Complementation assays. Genotyping of the T0 lines using Cleaved Amplified Polymorphic Sequences (CAPS) markers. Leaves were photographed at 21 days post sowing (dps). For results of agarose gel electrophoresis, one band indicates the *rbl1* mutant and three bands a complementation line. Bar, 1 cm. **g**, qRT-PCR assays of *RBL1* in the WT, *rbl1*, and complementation lines. Complementation line 10 was used as CoR1 in Figure 1. Gene *Actin* was used as the internal control. Bars in (**c**), (**d**), and (**g**) indicate standard deviations, and asterisks indicate significant differences compared to the WT using the unpaired Student’s *t*-test (*$P < 0.05$, **$P < 0.01$, ***$P < 0.001$, ****$P < 0.0001$).

Extended Data Fig. 3 | Expression assays of *RBL1*.

a, qRT-PCR assays of *RBL1* in different tissues of the wild-type (WT, Kitaake) plants at the flowering stage. **b**, qRT-PCR assays of *RBL1* in response to rice blast at the seedling stage of Kitaake. Kitaake

plants spray-inoculated with *M. oryzae* strain ZB25 were used in the assay. **c**, Tissue-specific expression of *RBL1* visualized by staining for the β-glucuronidase (GUS) activity under control of the *RBL1* promoter in the reporter line. For numbers: 1, seedling; 2 and 3, root; 4, stem; 5, shoot apical mristem; 6, leaf; 7, stamen; 8, pistil; 9, premilk stage; 10, panicle; 11, maturity stage. Bars in 1, 4, and 7, 5 mm; bars in 2, 3, 5, 6, and 8 to 11, 1 mm. Bars indicate standard deviations. Significant differences indicated by different letters were calculated using the Duncan's new multiple range test.

Extended Data Fig. 4 | The *Arabidopsis thaliana cds* mutants show enhanced resistance to *Phytophthora capsica.*

a, Phylogenetic analysis of RBL1 homologs from plants and other organisms. The phylogenetic tree was constructed using MEGA10. Accession numbers for different RBL1 homologs: *Arabidopsis thaliana* (NP_176433.2), *Beta vulgaris subsp. vulgaris* (XP_010694835.1), *Brachypodium distachyon* (XP_003564318.1), *Brassica rapa* (RID78417.1), *Chenopodium quinoa* (XP_021731901.1), *Chlamydomonas reinhardtii* (PNW85433.1), *Glycine max* (XP_003556374.1), *Gossypium barbadense* (KAB2026876.1), *Homo sapiens* (NP_001254.2), *Hordeum vulgare* (KAE8818711.1), *Mus musculus* (NP_775546.2), *Oryza sativa* (NC_029256.1), *Saccharomyces cerevisiae* (AJQ02739.1), *Schizosaccharomyces pombe* (NP_596416.1), *Sorghum bicolor* (KAG0539475.1), *Triticum aestivum* (KAF7023922.1), and *Zea mays* (NP_001132909.1). **b**, Protein domain analysis of RBL1 homologs from various organisms. Conserved domains in RBL1 homologs were predicted using the Evolve program. CTP_transf_1, phosphatide cytidylyltransferase. **c**, Amino acid alignment of the 19 residues that are truncated in the *rbl1* line. The consensus is shown at the bottom. **d**, The *cds* mutant and the wild-type (WT, Col-0, *A. thaliana*) plants at 28 days post sowing (dps). Bar, 1 cm. **e**, qRT-PCR assays. Total RNA was extracted from leaves of 4-week-old plants. **f**, Leaf length of the WT and *cds* mutant lines at 28 dps. **g-i**, Infected leaves (**g**), lesion area (**h**), and relative quantification of pathogen biomass (**i**) of inoculated WT and *cds* lines at 36 hours post-inoculation (hpi) with *Phytophthora capsica* strain LT263. Bar, 1 cm. Data are displayed as box and whisker plots with individual data points. The box plot elements are: center line, median; box limits, 25th and 75th percentiles. Significant differences indicated by different letters were calculated using the Duncan's new multiple range test.

Extended Data Fig. 5 | Exogenous supplementation of PI delays lesion formation in *rbl1*.

a, Lesion formation was suppressed in the *rbl1* but not *cul3a* or *spl-D* mutants. Plants were grown on the 1/2 MS media supplemented with PI. WT, the wild-type Kitaake. Photographs were taken from 12-day-old *rbl1*, 2-week-old *clu3a*, and 2-week-old *spl-D* plants with corresponding control lines. Bar, 1 cm. **b**, Lesion formation in the *rbl1* mutant was not affected by application of exogenous PG. Plants were grown on the 1/2 MS media supplemented with PG. Photographs were taken from 12-day-old plants. Bar, 1 cm. **c**, Lesion formation in the *rbl1* mutant was enhanced with exogenous application of $PI(4,5)P_2$. Plants

were grown on the 1/2 MS media supplemented with $PI(4,5)P_2$. Photographs were taken from 10-day-old plants. Bar, 1 cm. **d**, Exogenous PA enhances lesion formation in *rbl1* and leaf tip necrosis in WT. Bar, 1 cm. **e**, Lesion formation in *rbl1* was suppressed by exogenous diphenyleneiodonium chloride (DPI). Plants were grown on the 1/2 MS media supplemented with DPI. Photographs were taken of 10-day-old plants. Bar, 1 cm. Bars indicate standard deviations, and asterisks indicate significant differences compared to the mock using the unpaired Student's *t*-test (*P < 0.05, **P < 0.01, ***P < 0.001, ****P < 0.0001).

Extended Data Fig. 6 | Design of gRNA multiplexing in genome editing of *RBL1* and field trials. **a**, Gene structure of *RBL1* and the site targeted by each numbered guide RNA (gRNA) for genome editing. **b**, Map and cloning sites of the CRISPR/Cas9 vector pRGEB32 used in genome editing (left); vectors with different gRNAs (right). **c**, Sequences of gRNAs designed using CRISPR-P 2.0. Purple letters indicate protospacer-adjacent motif sites (PAMs). **d**, A schematic diagram of co-transformation of different constructs and genotyping of T0 lines. Edited sites in each T0 plant were identified using Sanger sequencing and agarose gel electrophoresis. WT, the wild-type Kitaake. **e**, Design of the normal field plots. **f**, Design of the field plots in the rice blast nursery. WT, the wild-type Kitaake; *RBL12*, the edited line; LTH, the very susceptible rice variety Lijiangxintuanheigu, which was used as the spreader line for rice blast. Each plot contains 100 plants 0.2 m apart. **g**, Identification of transgene-free T1 plants of *RBL12*. Primers specific to the *Cas9*, *hph* and *Actin* genes, respectively, were used in genotyping. The *hph* gene encoding a hygromycin B phosphotransferase confers hygromycin resistance for rice transgenic lines. The amplicon of the *Actin* gene was used as the DNA quality control. WT, Kitaake. **h.** Agronomic traits of the *RBL12* and Kitaake lines. Data for each agronomic trait were collected from 50 plants for each line that was grown in the normal paddy field. In the box and whisker plots, dots indicate individual data points, and the error bars represent maximum and minimum values. Center line, median; box limits, 25th and 75th percentiles. Asterisks indicate significant differences using the unpaired Student's *t*-test (***P < 0.001).

Extended Data Fig. 7 | Systematic characterization of the *RBL12* line and the allele. **a**, Sanger sequencing of the edited site indicated by the arrow in the *RBL12* line with the wild-type (WT, Kitaake) as the reference. The PAM site was shown in blue, and the dashed line represents the 12-bp deletion. **b**, Amino acid sequence alignment of RBL1 homologs around the four residues (underlined) that are truncated in the *RBL12* line. Highlighted are conserved residues in the RBL1 homologs. **c**, ROS generation in the WT, *RBL12*, Nipponbare (Nip), LTH, and R498 rice plants challenged with chitin at the booting stage. RLU, relative light unit. **d**, qRT-PCR assays of *RBL1* expression in different tissues of the WT, *RBL12*, and *rbl1* plants at the flowering stage. **e**, qRT-PCR assays of heterologous expression of *RBL1* in yeast. Yeast 18s rRNA was used as the internal control. **f**, Immunoblotting analysis of RBL1-,

rbl1-, and RBL12-6×His fusion proteins in yeast. Ponceau S staining indicates the protein loading. WT, yeast strain BY4741; other strains are transformants of the yeast *cds1* mutant carrying pYES2-*RBL1,* pYES2-*rbl1*, and pYES2-*RBL12,* respectively. **g**, Stability of the RBL1- and RBL12-6×His fusion proteins analyzed using differential scanning calorimetry (DSC). **h**, Subcellular localization of the RBL1- and RBL12-GFP fusion proteins transiently expressed in *Nicotiana benthamiana* leaf epidermal cells, analyzed together with the endoplasmic reticulum marker HDEL-mCherry. Bars, 25 μm. **i**, RBL1-GFP rescues the growth defect of yeast *cds1*. WT, yeast strain BY4741; R1G, the yeast *cds1* mutant carrying pYES2-*RBL1*-GFP. Strains were cultured on YPGal or YPD plates at 30°C for 3 days before sampling. Immunoblotting analysis of the RBL1-GFP fusion protein in the yeast strain R1G that forms a homodimer. CBB staining indicates the protein loading. **j**, 9-week-old WT, *RBL12*, and complemented T1 plants. The white asterisk indicates the spontaneous lesion in the insets. Bar, 10 cm. Shown on the right are qRT-PCR assays of *RBL1* in the WT, *RBL12*, and CoR1-*RBL12* lines. Gene *Actin* was used as the internal control. **k**, Punch inoculation of the WT, *RBL12*, and CoR1-*RBL12* lines with *M. oryzae*. The lesion area was measured at 14 dpi. Bar, 1 cm. **l**, Leaves of 3-week-old WT, *rbl1*, *RBL12*, and F1 plants of *rbl1* crossed with *RBL12*. Bar, 1 cm. **m**, The WT, *RBL12*, and F2 plants derived from the WT line crossed with *RBL12* at 60 dps. Spontaneous lesions-indicated by white asterisks-formed on the top leaves of homozygous *RBL12* lines. Bars, 10 cm. **n**, Punch inoculation assays of the WT, *RBL12*, and F2 plants with *M. oryzae*. The lesion area was measured at 14 dpi. Bar, 1 cm. **o**, qRT-PCR assays of *RBL1* in the WT, *RBL12* and F2 plants at the tillering stage. **p**, WT and *RBl12* transgenic plants expressing the PI(4,5)P_2 biosensor at 32 hpi with *M. oryzae* stain ZB25 expressing the cytoplasmic effector Pwl2 tagged with mCherry. BIC, biotrophic interfacial complex; EIHM, extra-invasive hyphal membrane; IH, invasive hyphae. Bar, 10 μm. **q**, BIC formation in plants shown in (**r**). **r**, Membrane lipid composition analysis of the WT, *RBL12*, and *rbl1* lines. DW, dry weight. **s**, PIP and PIP_2 content in the WT, *RBL12*, and *rbl1* lines. The box plot elements are: center line, median; box limits, 25th and 75th percentiles. Bars in (**e**), (**j**), (**q**), (**r**), and (**s**) indicate standard deviations, and asterisks in (**e**) and (**q**) indicate significant differences using the unpaired Student's *t*-test (***P* < 0.01). Significant differences indicated by different letters in (**d**), (**j**), (**k**), (**n**), (**o**), (**r**), and (**s**) were calculated using the Duncan's new multiple range test.

Extended Data Fig. 8 | Genome editing of *RBL1* enhances disease resistance in two other rice cultivars.

a, Lesion mimic phenotypes and enhanced resistance to *M. oryzae* in *RBL1*-edited Nipponbare (Nip) lines. Infected leaves and lesion area of punch-inoculated *RBL1*-edited lines with *M. oryzae* at 14 dpi. Bar, 1 cm. **b**, 12-week-old *RBL1*-edited Nipponbare lines. Bar, 10 cm. **c**, qRT-PCR assays of *RBL1* and plant defense-related genes *OsPR8* and *OsPR10* in the *RBL1*-edited Nipponbare lines. Total RNA was

extracted from 4-week-old leaves. The *Actin* gene was used as the internal control. **d-f**, Similar assays as shown in (**a-c**) were performed on one local rice cultivar Zhonghua11 (ZH11). **g**, Sanger sequencing of the edited sites, indicated by arrows, in *nr-7* and *zr-7* lines, with the wild-type (WT, Kitaake) as the reference. The mutated nucleotides are shown in gray (deletion) and blue (insertion). **h**, Amino acid sequence alignment of the region mutated in lines *nr-7* and *zr*-7. The four amino acids truncated in RBL12 are indicated by asterisks. Shaded are conserved residues in the RBL1 homologs. Two amino acids are truncated in *nr-7*, with the first one overlapping the truncated region in RBL12. An 84-bp frameshift mutation caused by a 1-bp deletion followed by a 1-bp insertion alters the sequence of 28 amino acids (gray) in *zr-7*, with the first two overlapping the truncated region in RBL12. Bars indicate standard deviations, and asterisks indicate significant differences compared to the WT using the unpaired Student's *t*-test (***$P < 0.001$, ****$P < 0.0001$). Significant differences indicated by different letters in (**c**) and (**f**) were calculated using the Duncan's new multiple range test.

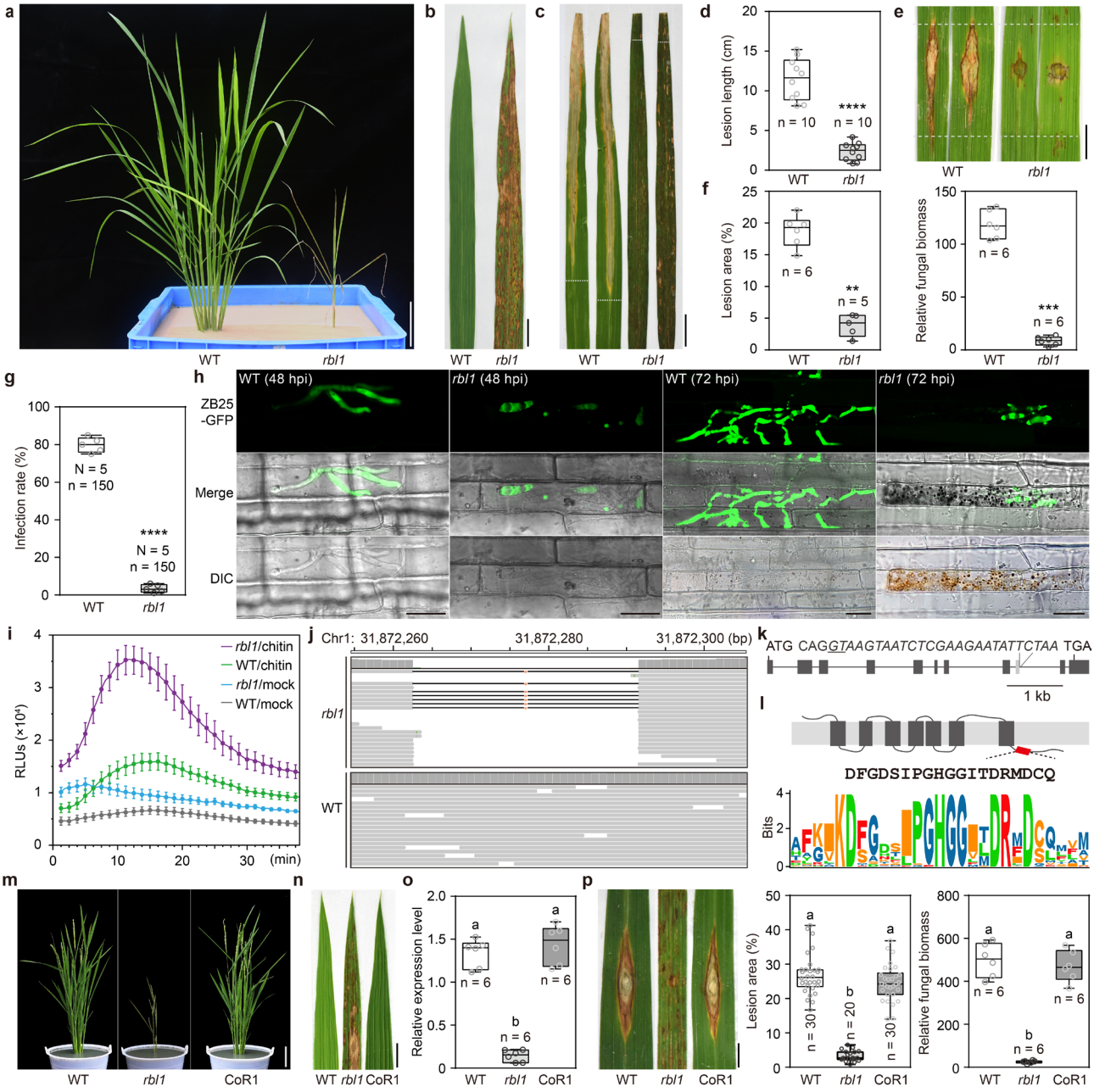

Fig.1 | Cloning of the *RBL1* gene from the lesion mimic mutant *rbl1*, which has enhanced immunity.

a, *rbl1* mutant and wild-type (WT, KitaakeX) plants at 40 days post sowing (dps). Bar, 10 cm. **b**, Spontaneous lesions. Bar, 1 cm, which is the same for other panels without specifications. **c**, Inoculation of rice lines with *Xoo* at 14 days post-inoculation (dpi) and lesion length (**d**). **e**, Punch inoculation with *M. oryzae* at 14 dpi. The dashed lines indicate the leaf area covered by aluminum foil before spontaneous lesions appeared. **f**, Lesion area and relative fungal biomass. **g**, Fungal infection rates at 72 hours post-inoculation (hpi). **h**, Rice sheath cells infected by eGFP-tagged *M. oryzae* strain ZB25. Bars, 25 μm. **i**, ROS generation in rice plants challenged with chitin and water (mock). **j**, Screenshot of the 29-bp deletion in *rbl1*. **k**, Gene structure of *RBL1*. The gray box indicates the exon skipped in *rbl1*. The sequence of the deletion is shown, and the intron sequence is italic with the intron recognition site *"GT"* underlined. **l**, The predicted secondary structure of RBL1. The red box indicates the truncation. The CDS signature motif is shown at the bottom. **m**, 10-week-old

WT, *rbl1*, and complemented (CoR1) plants. Bar, 10 cm. **n**, Leaves of the lines in (**m**). **o**, qRT-PCR assays of *RBL1*. **p**, Infected leaves, lesion area and relative fungal biomass of rice lines with *M. oryzae* at 14 dpi. Data are displayed as box and whisker plots with individual data points: center line, median; box limits, 25th and 75th percentiles. Asterisks indicate significant differences using the unpaired Student's *t*-test (***P* < 0.01, ****P* < 0.001, *****P* < 0.0001). Significant differences indicated by different letters in (**o**) and (**p**) were calculated using the Duncan's new multiple range test.

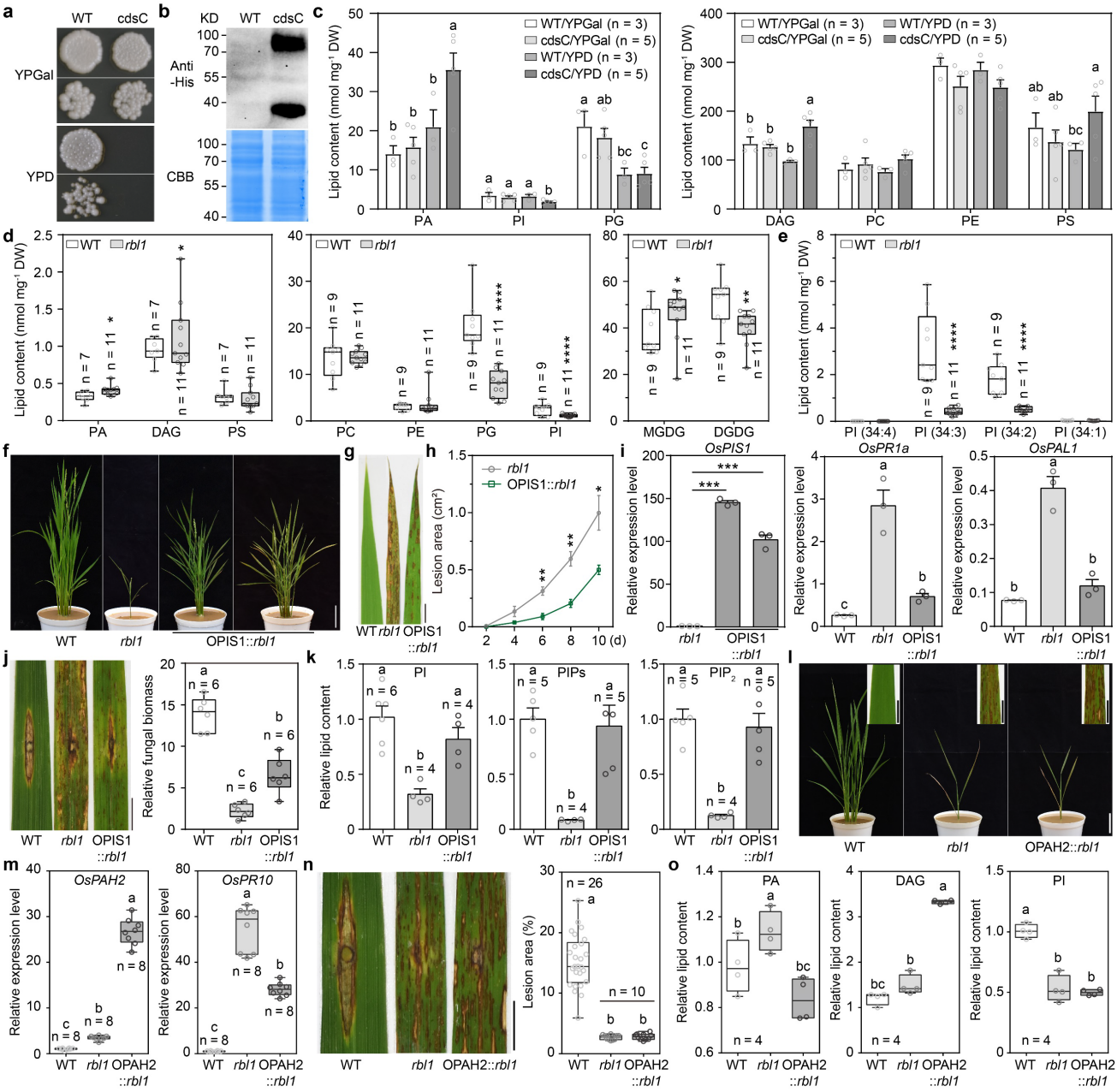

Fig.2 | RBL1 functions as a CDP-DAG synthase.

a, *RBL1* rescues the growth defect of the yeast *cds1* mutant. WT, yeast strain BY4741; cdsC, yeast mutant *cds1* expressing *RBL1*. **b**, Immunoblotting analysis of the RBL1-6×His fusion protein (monomeric and dimeric states). CBB, Coomassie brilliant blue. **c**, Lipidomics assays of yeast strains cultured in YPGal or YPD. **d**, Lipidomic analysis of the 4-week-old wild-type (WT, Kitaake) and *rbl1* lines. DW, dry weight. **e**, Fatty acid species of PI. No alterations were detected between WT and *rbl1* for fatty acid species 36:1 to 36:6. **f**, 8-week-old T1 plants of the *OsPIS1* overexpression OPIS1::*rbl1* lines. Bar, 10 cm. **g**, Lesions on new rice leaves. Bar, 1 cm. **h**, Lesion area of the lines in (**g**). **i**, qRT-PCR assays of genes in the OPIS1::*rbl1* line. **j**, Punch inoculation with *M. oryzae* and relative fungal biomass at 14 dpi. Bar, 1 cm. **k**, PI, PIP, and PIP_2 assays. **l**, 8-week-old plants. OPAH2::*rbl1*, the *rbl1* line overexpressing *OsPAH2*. Black bar, 1 cm; white bar, 10 cm. **m**, qRT-PCR assays. **n**, Punch inoculation with *M. oryzae* and the lesion area at 14 dpi. Bar, 1 cm. **o**,

Lipidomics assays of different rice lines. The box plot elements are: center line, median; box limits, 25th and 75th percentiles. Bars in (**c**), (**h**), (**i**), and (**k**) indicate standard deviations, and asterisks in (**d**), (**e**), (**h**), and (**i**) indicate significant differences using the unpaired Student's *t*-test (*$P < 0.05$, **$P < 0.01$, ***$P < 0.001$, ****$P < 0.0001$). Significant differences indicated by different letters in (**c**), (**i**), (**j**), (**k**), (**m**), (**n**), and (**o**) were calculated using the Duncan's new multiple range test.

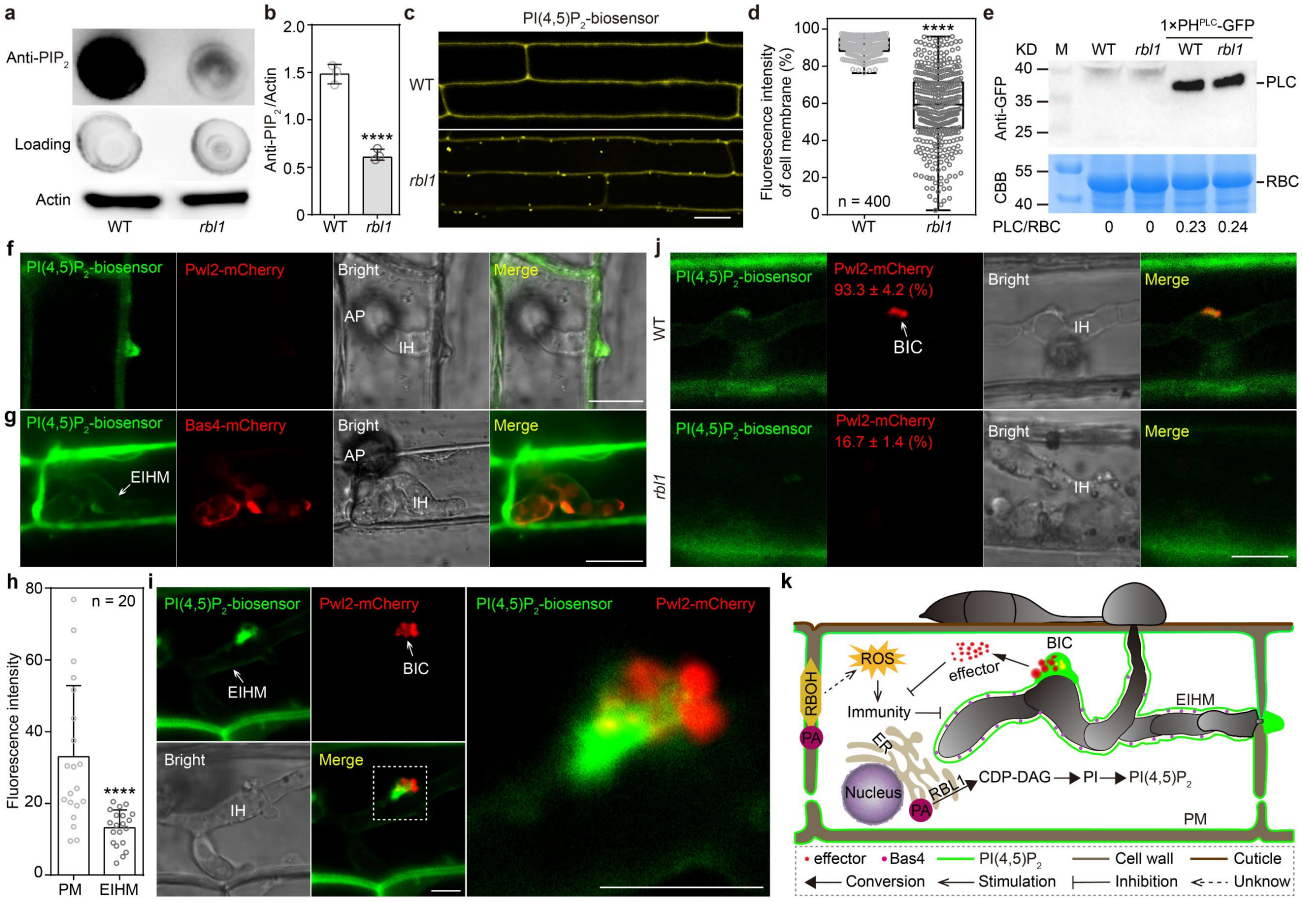

Fig. 3 | PI(4,5)P₂, enriched in infection-specific structures, is reduced in *rbl1* plants.

a, Dot blotting of membrane PIP_2 in the wild-type (WT, Kitaake) and *rbl1* lines. **b**, The relative levels of membrane PIP_2. **c**, Epidermal cells of rice lines expressing the $PI(4,5)P_2$ biosensor. Bar, 25 μm. **d**, Relative fluorescence intensity of the $PI(4,5)P_2$ biosensor in (**c**). The box plot elements are: center line, median; box limits, 25th and 75th percentiles. **e**, Immunoblotting of the $PI(4,5)P_2$ biosensor in (**c**). PLC, the biosensor; RBC, ribulose-1,5-bis-phosphate carboxylase/oxygenase. **f**, $PI(4,5)P_2$ aggregates around the infectious hyphal tip of *M. oryzae* at 22 hpi. AP, appressorium; IH, invasive hyphae. Pwl2 is a cytoplasmic effector, a biomarker for the biotrophic interfacial complex (BIC). **g**, Rice cells of the WT expressing the $PI(4,5)P_2$ biosensor infected by the *M. oryzae* strain expressing the apoplastic effector Bas4 tagged with the mCherry protein at 27 hpi. EIHM, extra-invasive hyphal membrane. Bar, 10 μm. **h**, Fluorescence intensity of the plasma membrane (PM) and EIHM shown in (**g**). **i**, $PI(4,5)P_2$ and Pwl2 at the BIC at 32 hpi. The inset shows the enlarged BIC. Bars, 5 μm. **j**, BIC formation in different rice lines. Bar, 10 μm. The numbers represent the BIC formation rates from 150 infected cells. **k**, Working model of RBL1 in rice resistance to *M. oryzae*. RBL1 is important for the biosynthesis of PI and PIPs including $PI(4,5)P_2$. As *M. oryzae* invades, $PI(4,5)P_2$ is recruited to the EIHM and enriched in BIC. Accumulation of PA is a minor factor of enhanced immunity of *rbl1*. Other unknown factors also contribute to enhanced immunity of *rbl1*. Bars in (**b**) and (**h**) indicate standard deviations, and asterisks indicate significant differences using the unpaired Student's *t*-test (****$P < 0.0001$).

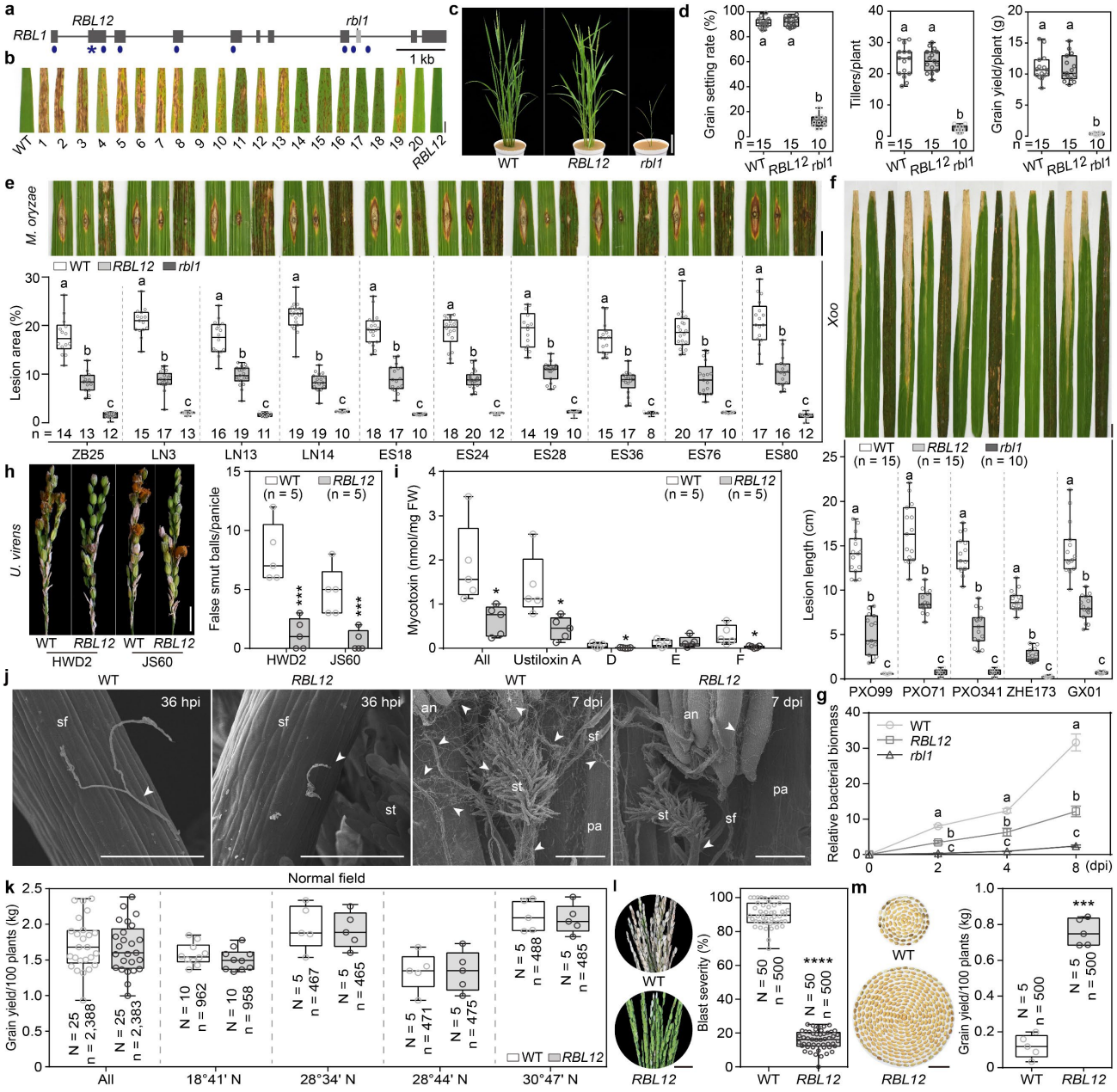

Fig.4 | *RBL12* confers broad-spectrum resistance with no observed yield penalty in field trials.

a, Guide RNA sites, indicated by dots, for genome editing of *RBL1*. The asterisk indicates the edited site in *RBL12*. **b**, *RBL1* edited lines. WT, Kitaake. Bar, 1 cm, which is the same for other panels without specifications. **c**, 8-week-old plants in the greenhouse. Bar, 10 cm. **d**, Agronomic traits. **e**, Lesions with *M. oryzae* at 14 dpi. **f**, Lesions with *Xoo* at 14 dpi. **g**, *In planta* bacterial growth of *Xoo* strain PXO99. **h**, Infected panicles with *U. virens*. Rice false smut balls were counted at 17 dpi. **i**, Quantitative assays of ustiloxins in infected panicles. FW, fresh weight. **j**, Infected spikelets with *U. virens*. Arrows indicate invasive hyphae. an, anther; pa, palea; sf, stamen filament; st, stigma. Bars, 100 μm. **k**, Rice grain yield in the "Normal" field trials with low incidence of rice blast. **l**, Field assessment of blast resistance in the blast nursery. Representative panicles are shown on the left. Disease severity is indicated by the percentage of necrotic panicles for each plant caused by *M. oryzae*. **m**, Grain yield of plants grown in the blast nursery. Seeds per plant are shown on the left.

The box plot elements are: center line, median; box limits, 25th and 75th percentiles. Asterisks in (**h**), (**i**), (**l**), and (**m**) indicate significant differences using the unpaired Student's *t*-test (*$P < 0.05$, ***$P < 0.001$, ****$P < 0.0001$). Significant differences indicated by different letters in (**d-g**) were calculated using the Duncan's new multiple range test.

Extended Data

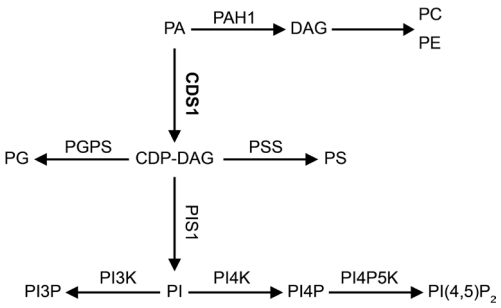

Extended Data Fig. 1 | The plant glycerolipid metabolic pathway related to cytidinediphosphate-diacylglycerol synthase 1 (CDS1).

Rice RBL1 is homologous to yeast Cds1. CDP-DAG, cytidinediphosphate-diacylglycerol; DAG, diacylglycerol; PA, phosphatidic acid; PAH, phosphatidic acid phosphohydrolase; PC, phosphatidylcholine; PE, phosphatidylethanolamine; PG, phosphatidylglycerol; PGPS, phosphatidylglycerol phosphate synthase; PI, phosphatidylinositol; PI4K, phosphatidylinositol 4-kinases; PI4P, phosphatidylinositol 4-phosphate; PI4P5K, phosphatidylinositol 4-phosphate 5-kinase; $PI(4,5)P_2$, phosphatidylinositol-4,5-bisphosphate; PIS1, phosphatidylinositol synthase; PS, phosphatidylserine; PSS, phosphatidylserine synthase.

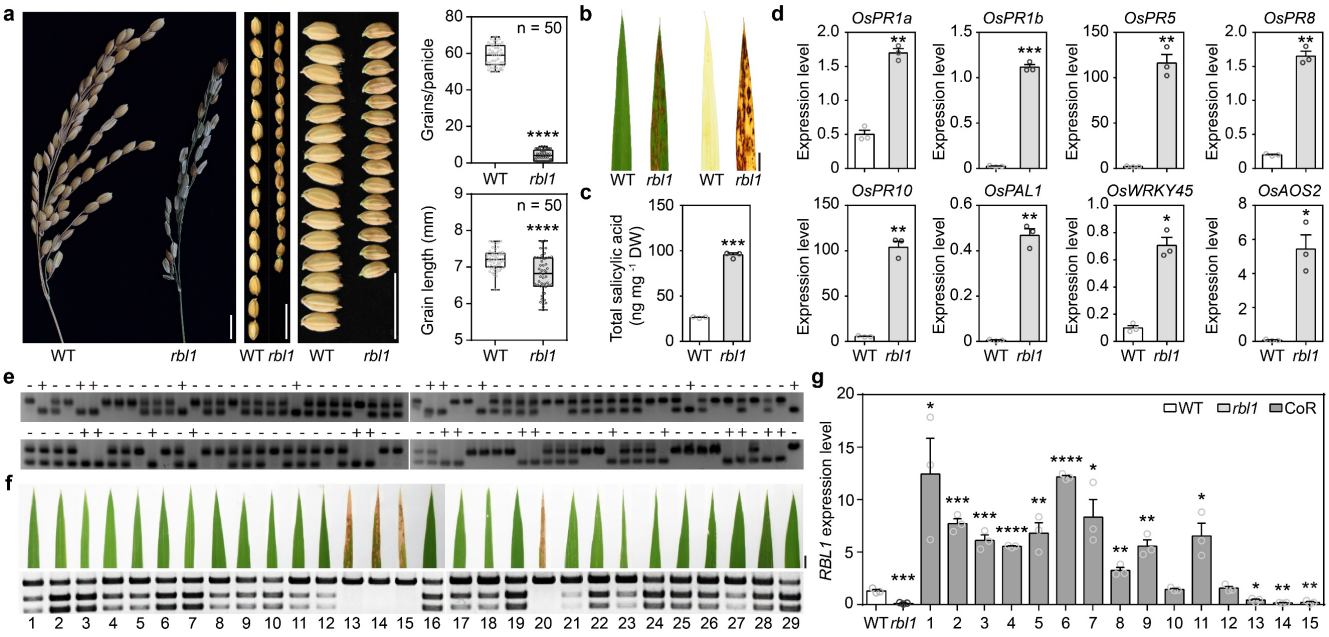

Extended Data Fig. 2 | Expression of plant defense-related genes, yield, and genetic complementation of the *rbl1* line.

a, Panicles and seeds of the *rbl1* and WT lines. Bars, 1 cm. Grain yield of the *rbl1* and WT lines. Data are displayed as box and whisker plots with individual data points. The box plot elements are: center line, median; box limits, 25th and 75th percentiles. **b**, *In situ* detection of reactive oxygen species (ROS) in the *rbl1* mutant and wild-type (WT, KitaakeX) leaves using 3,3'-diaminobenzidine (DAB) staining. Bar, 1 cm. **c**, The total salicylic acid (SA) level is increased in the *rbl1* mutant. Total SA was isolated from leaves of 2-week-old seedlings. **d**, qRT-PCR assays of marker genes of plant immunity. Total RNA was extracted from leaves of 4-week-old plants. Gene *Actin* was used as the internal control. **e**, A 29-bp deletion cosegregates with the lesion mimic phenotype in the M3 population of line *rbl1*. PCR results of InDel markers targeting the 29-bp deletion: one short band, homozygous; one large band, wild-type alleles; two bands, heterozygous. "+" indicates lesions on the leaf of the M3 plant and "-" no lesion. A $\chi 2$ test of the phenotypic ratio revealed that the actual value 26: 92 of lesioned plants to normal plants is statistically similar to the expected value 1: 3 ($\chi 2 = 0.213$, P-value = 0.644 > 0.05). **f**, Complementation assays. Genotyping of the T0 lines using Cleaved Amplified Polymorphic Sequences (CAPS) markers. Leaves were photographed at 21 days post sowing (dps). For results of agarose gel electrophoresis, one band indicates the *rbl1* mutant and three bands a complementation line. Bar, 1 cm. **g**, qRT-PCR assays of *RBL1* in the WT, *rbl1*, and complementation lines. Complementation line 10 was used as CoR1 in Figure 1. Gene *Actin* was used as the internal control. Bars in (**c**), (**d**), and (**g**) indicate standard deviations, and asterisks indicate significant differences compared to the WT using the unpaired Student's *t*-test (*$P < 0.05$, **$P < 0.01$, ***$P < 0.001$, ****$P < 0.0001$).

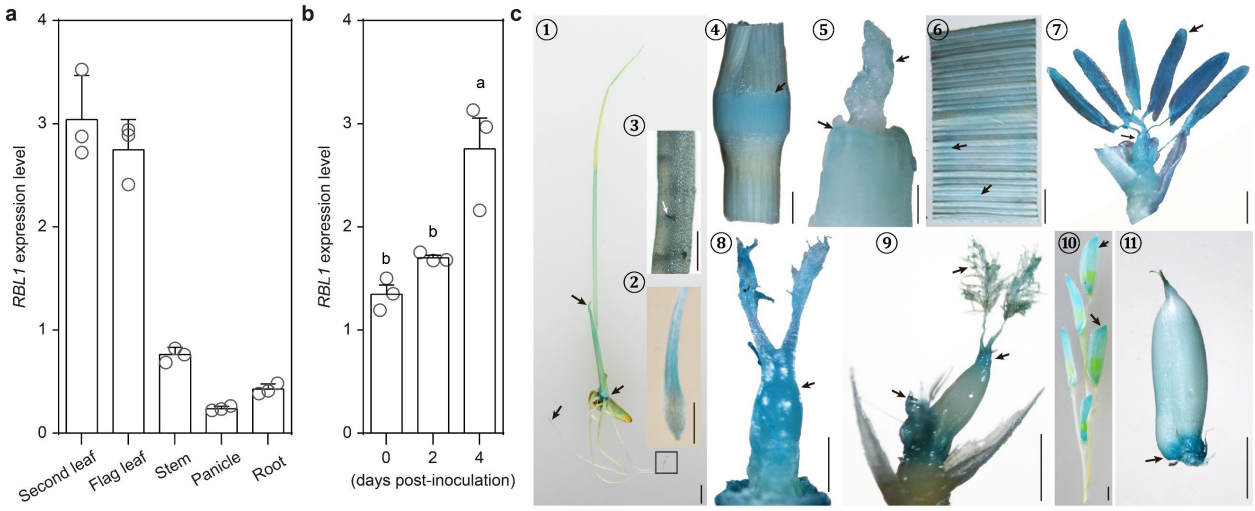

Extended Data Fig. 3 | Expression assays of *RBL1*.

a, qRT-PCR assays of *RBL1* in different tissues of the wild-type (WT, Kitaake) plants at the flowering stage. **b**, qRT-PCR assays of *RBL1* in response to rice blast at the seedling stage of Kitaake. Kitaake plants spray-inoculated with *M. oryzae* strain ZB25 were used in the assay. Significant differences indicated by different letters were calculated using the Duncan's new multiple range test. **c**, Tissue-specific expression of *RBL1* visualized by staining for the β-glucuronidase (GUS) activity under control of the *RBL1* promoter in the reporter line. For numbers: 1, seedling; 2 and 3, root; 4, stem; 5, shoot apical mristem; 6, leaf; 7, stamen; 8, pistil; 9, premilk stage; 10, panicle; 11, maturity stage. Bars in 1, 4, and 7, 5 mm; bars in 2, 3, 5, 6, and 8 to 11, 1 mm.

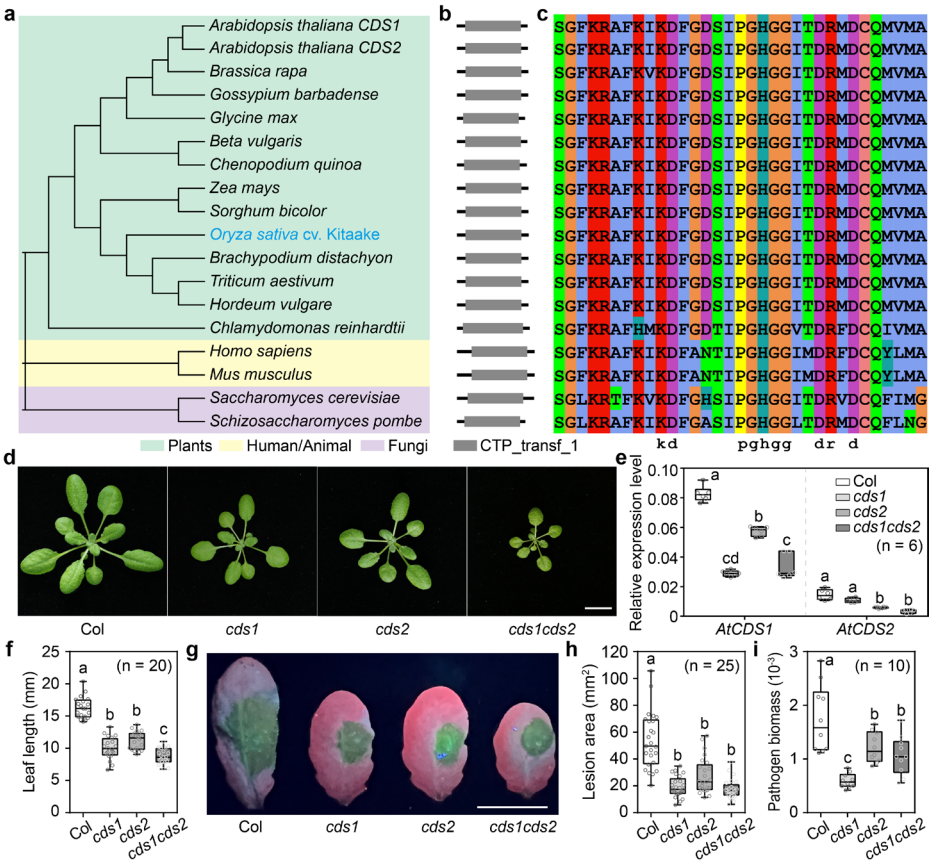

Extended Data Fig. 4 | The *Arabidopsis thaliana cds* mutants show enhanced resistance to *Phytophthora capsica*. **a**, Phylogenetic analysis of RBL1 homologs from plants and other organisms. The phylogenetic tree was constructed using MEGA10. Accession numbers for different RBL1 homologs: *Arabidopsis thaliana* (NP_176433.2), *Beta vulgaris subsp. vulgaris* (XP_010694835.1), *Brachypodium distachyon* (XP_003564318.1), *Brassica rapa* (RID78417.1), *Chenopodium quinoa* (XP_021731901.1), *Chlamydomonas reinhardtii* (PNW85433.1), *Glycine max* (XP_003556374.1), *Gossypium barbadense* (KAB2026876.1), *Homo sapiens* (NP_001254.2), *Hordeum vulgare* (KAE8818711.1), *Mus musculus* (NP_775546.2), *Oryza sativa* (NC_029256.1), *Saccharomyces cerevisiae* (AJQ02739.1), *Schizosaccharomyces pombe* (NP_596416.1), *Sorghum bicolor* (KAG0539475.1), *Triticum aestivum* (KAF7023922.1), and *Zea mays* (NP_001132909.1). **b**, Protein domain analysis of RBL1 homologs from various organisms. Conserved domains in RBL1 homologs were predicted using the Evolve program. CTP_transf_1, phosphatide cytidylyltransferase. **c**, Amino acid alignment of the 19 residues that are truncated in the *rbl1* line. The consensus is shown at the bottom. **d**, The *cds* mutant and the wild-type (WT, Col-0, *A. thaliana*) plants at 28 days post sowing (dps). Bar, 1 cm. **e**, qRT-PCR assays. Total RNA was extracted from leaves of 4-week-old plants. **f**, Leaf length of the WT and *cds* mutant lines at 28 dps. **g-i**, Infected leaves (**g**), lesion area (**h**), and relative quantification of pathogen biomass (**i**) of inoculated WT and *cds* lines at 36 hours post-inoculation (hpi) with *Phytophthora capsica* strain LT263. Bar, 1 cm. Data are displayed as box and whisker plots with individual data points. The box plot elements are: center line, median; box limits, 25th and 75th percentiles. Significant differences indicated by different letters were calculated using the Duncan's new multiple range test.

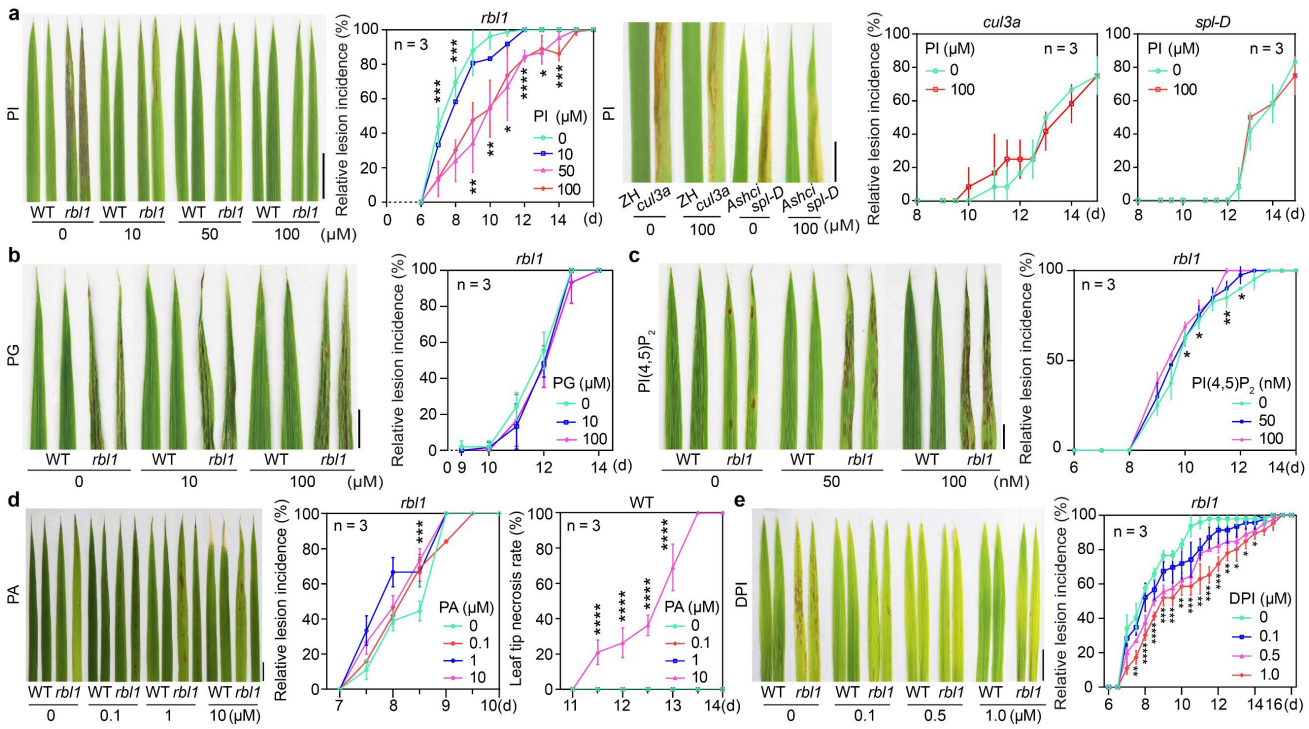

Extended Data Fig. 5 | Exogenous supplementation of PI delays lesion formation in *rbl1*.

a, Lesion formation was suppressed in the *rbl1* but not *cul3a* or *spl-D* mutants. Plants were grown on the 1/2 MS media supplemented with PI. WT, the wild-type Kitaake. Photographs were taken from 12-day-old *rbl1*, 2-week-old *clu3a*, and 2-week-old *spl-D* plants with corresponding control lines. Bar, 1 cm. **b**, Lesion formation in the *rbl1* mutant was not affected by application of exogenous PG. Plants were grown on the 1/2 MS media supplemented with PG. Photographs were taken from 12-day-old plants. Bar, 1 cm. **c**, Lesion formation in the *rbl1* mutant was enhanced with exogenous application of $PI(4,5)P_2$. Plants were grown on the 1/2 MS media supplemented with $PI(4,5)P_2$. Photographs were taken from 10-day-old plants. Bar, 1 cm. **d**, Exogenous PA enhances lesion formation in *rbl1* and leaf tip necrosis in WT. Bar, 1 cm. **e**, Lesion formation in *rbl1* was suppressed by exogenous diphenyleneiodonium chloride (DPI). Plants were grown on the 1/2 MS media supplemented with DPI. Photographs were taken of 10-day-old plants. Bar, 1 cm.

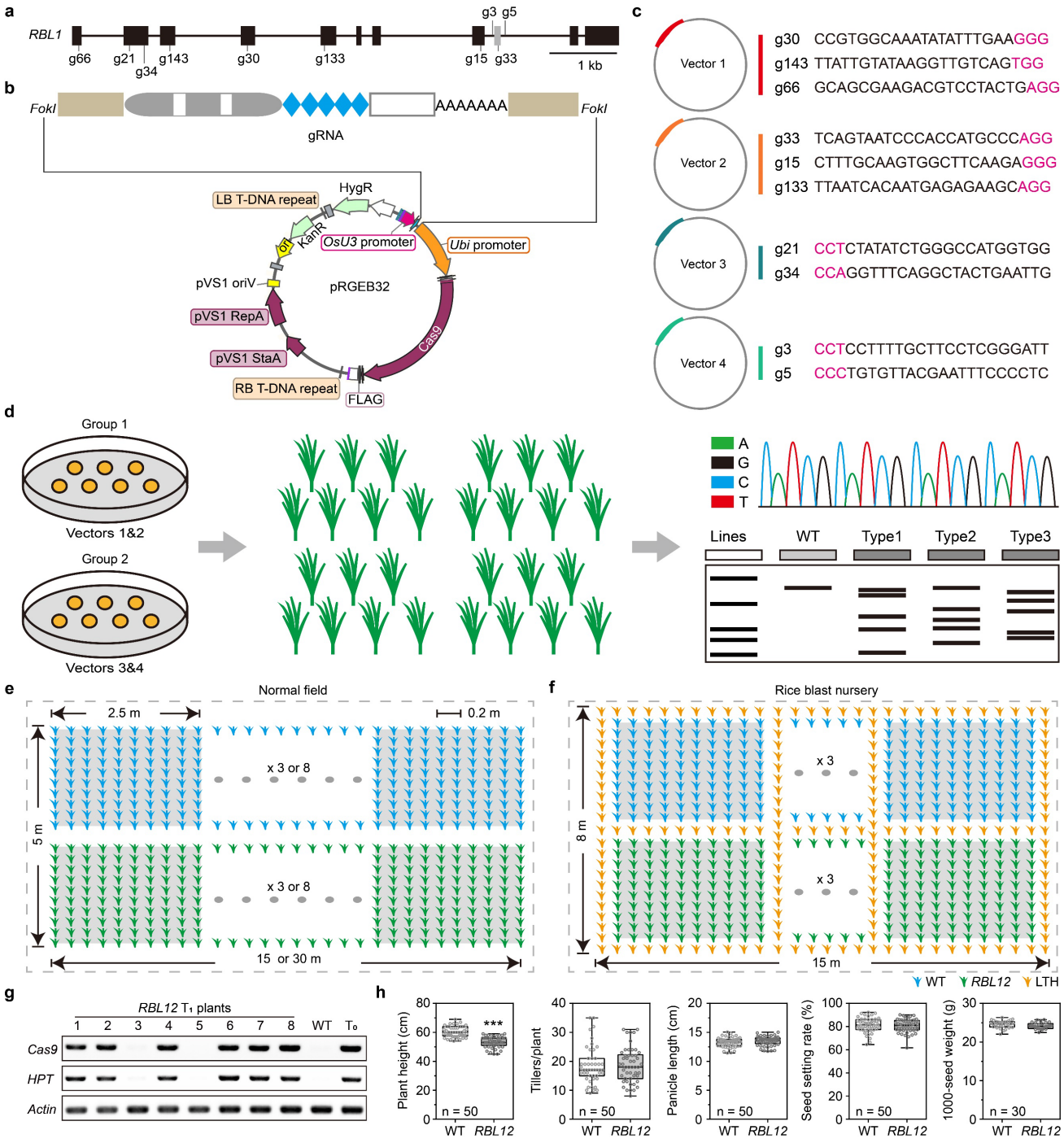

Extended Data Fig. 6 | Design of gRNA multiplexing in genome editing of *RBL1* and field trials.

a, Gene structure of *RBL1* and the site targeted by each numbered guide RNA (gRNA) for genome editing. **b**, Map and cloning sites of the CRISPR/Cas9 vector pRGEB32 used in genome editing (left); vectors with different gRNAs (right). **c**, Sequences of gRNAs designed using CRISPR-P 2.0. Purple letters indicate protospacer-adjacent motif sites (PAMs). **d**, A schematic diagram of co-transformation of different constructs and genotyping of T0 lines. Edited sites in each T0 plant were identified using Sanger sequencing and agarose gel electrophoresis. WT, the wild-type Kitaake. **e**, Design of the normal field plots. **f**, Design of the field plots in the rice blast nursery. WT, the wild-type Kitaake; *RBL12*, the edited line; LTH, the very susceptible rice variety Lijiangxintuanheigu, which was used as the spreader line for rice blast. Each plot

contains 100 plants 0.2 m apart. **g**, Identification of transgene-free T1 plants of *RBL12*. Primers specific to the *Cas9*, *hph* and *Actin* genes, respectively, were used in genotyping. The *hph* gene encoding a hygromycin B phosphotransferase confers hygromycin resistance for rice transgenic lines. The amplicon of the *Actin* gene was used as the DNA quality control. WT, Kitaake. **h.** Agronomic traits of the *RBL12* and Kitaake lines. Data for each agronomic trait were collected from 50 plants for each line that was grown in the normal paddy field. In the box and whisker plots, dots indicate individual data points, and the error bars represent maximum and minimum values. Center line, median; box limits, 25th and 75th percentiles. Asterisks indicate significant differences using the unpaired Student's *t*-test (***$P < 0.001$).

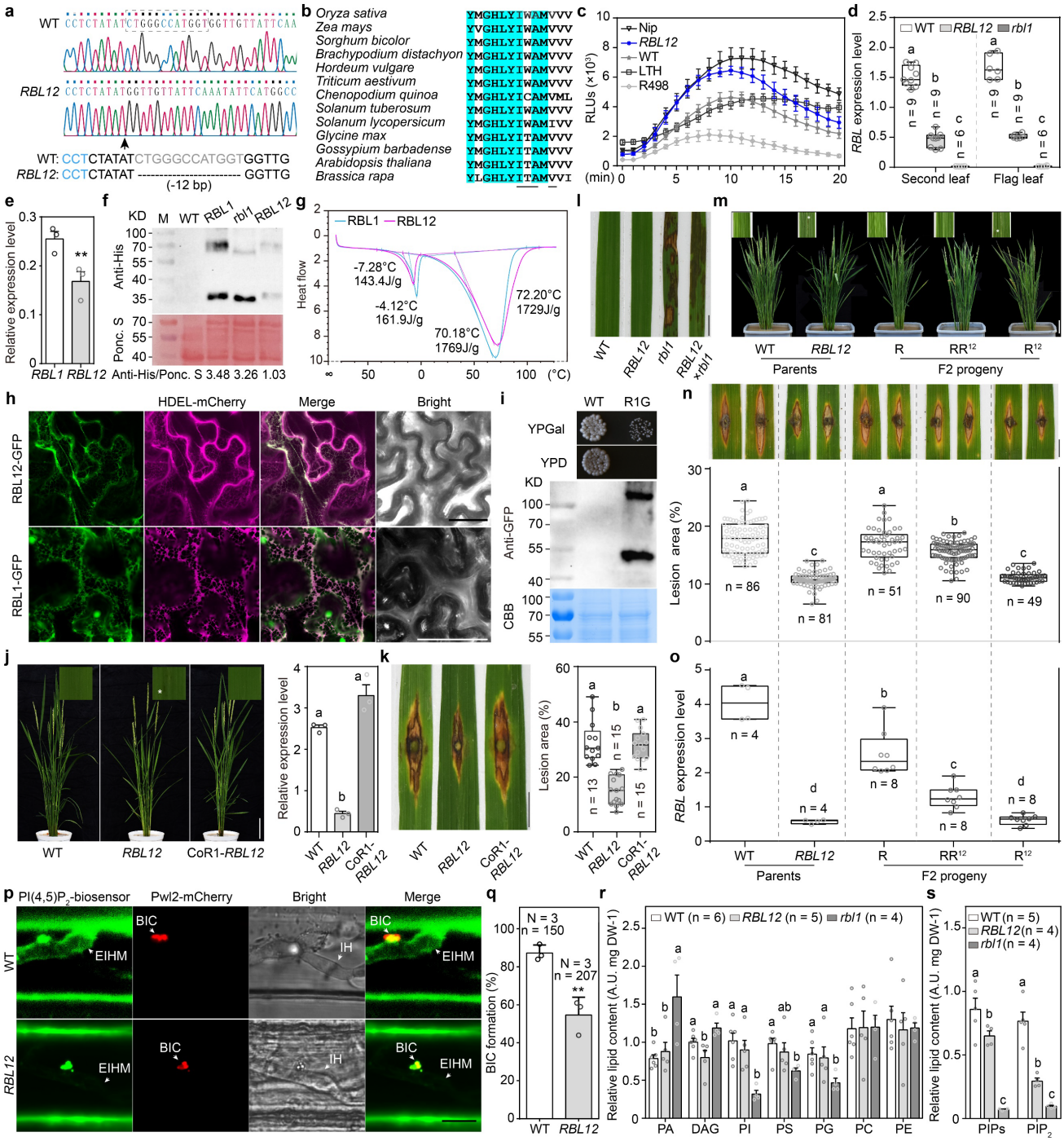

Extended Data Fig. 7 | Systematic characterization of the *RBL12* line and the allele.

a, Sanger sequencing of the edited site indicated by the arrow in the *RBL12* line with the wild-type (WT, Kitaake) as the reference. The PAM site was shown in blue, and the dashed line represents the 12-bp deletion. **b**, Amino acid sequence alignment of RBL1 homologs around the four residues (underlined) that are truncated in the *RBL12* line. Highlighted are conserved residues in the RBL1 homologs. **c**, ROS generation in the WT, *RBL12*, Nipponbare (Nip), LTH, and R498 rice plants challenged with chitin at the booting stage. RLU, relative light unit. **d**, qRT-PCR assays of *RBL1* expression in different tissues of the WT, *RBL12*, and *rbl1* plants at the flowering stage. **e**, qRT-PCR assays of heterologous expression of *RBL1* in yeast. Yeast 18s rRNA was used as the internal control. **f**, Immunoblotting analysis of RBL1-, rbl1-, and

RBL12-6×His fusion proteins in yeast. Ponceau S staining indicates the protein loading. WT, yeast strain BY4741; other strains are transformants of the yeast *cds1* mutant carrying pYES2-*RBL1,* pYES2-*rbl1*, and pYES2-*RBL12,* respectively. **g**, Stability of the RBL1- and RBL12-6×His fusion proteins analyzed using differential scanning calorimetry (DSC). **h**, Subcellular localization of the RBL1- and RBL12-GFP fusion proteins transiently expressed in *Nicotiana benthamiana* leaf epidermal cells, analyzed together with the endoplasmic reticulum marker HDEL-mCherry. Bars, 25 μm. **i**, RBL1-GFP rescues the growth defect of yeast *cds1*. WT, yeast strain BY4741; R1G, the yeast *cds1* mutant carrying pYES2-*RBL1*-GFP. Strains were cultured on YPGal or YPD plates at 30°C for 3 days before sampling. Immunoblotting analysis of the RBL1-GFP fusion protein in the yeast strain R1G that forms a homodimer. CBB staining indicates the protein loading. **j**, 9-week-old WT, *RBL12*, and complemented T1 plants. The white asterisk indicates the spontaneous lesion in the insets. Bar, 10 cm. Shown on the right are qRT-PCR assays of *RBL1* in the WT, *RBL12*, and CoR1-*RBL12* lines. Gene *Actin* was used as the internal control. **k**, Punch inoculation of the WT, *RBL12*, and CoR1-*RBL12* lines with *M. oryzae*. The lesion area was measured at 14 dpi. Bar, 1 cm. **l**, Leaves of 3-week-old WT, *rbl1*, *RBL12*, and F1 plants of *rbl1* crossed with *RBL12*. Bar, 1 cm. **m**, The WT, *RBL12*, and F2 plants derived from the WT line crossed with *RBL12* at 60 dps. Spontaneous lesions-indicated by white asterisks-formed on the top leaves of homozygous *RBL12* lines. Bars, 10 cm. **n**, Punch inoculation assays of the WT, *RBL12*, and F2 plants with *M. oryzae*. The lesion area was measured at 14 dpi. Bar, 1 cm. **o**, qRT-PCR assays of *RBL1* in the WT, *RBL12* and F2 plants at the tillering stage. **p**, WT and *RBl12* transgenic plants expressing the $PI(4,5)P_2$ biosensor at 32 hpi with *M. oryzae* stain ZB25 expressing the cytoplasmic effector Pwl2 tagged with mCherry. BIC, biotrophic interfacial complex; EIHM, extra-invasive hyphal membrane; IH, invasive hyphae. Bar, 10 μm. **q**, BIC formation in plants shown in (**r**). **r**, Membrane lipid composition analysis of the WT, *RBL12*, and *rbl1* lines. DW, dry weight. **s**, PIP and PIP_2 content in the WT, *RBL12*, and *rbl1* lines. The box plot elements are: center line, median; box limits, 25th and 75th percentiles. Bars in (**e**), (**j**), (**q**), (**r**), and (**s**) indicate standard deviations, and asterisks in (**e**) and (**q**) indicate significant differences using the unpaired Student's *t*-test (***P* < 0.01). Significant differences indicated by different letters in (**d**), (**j**), (**k**), (**n**), (**o**), (**r**), and (**s**) were calculated using the Duncan's new multiple range test.

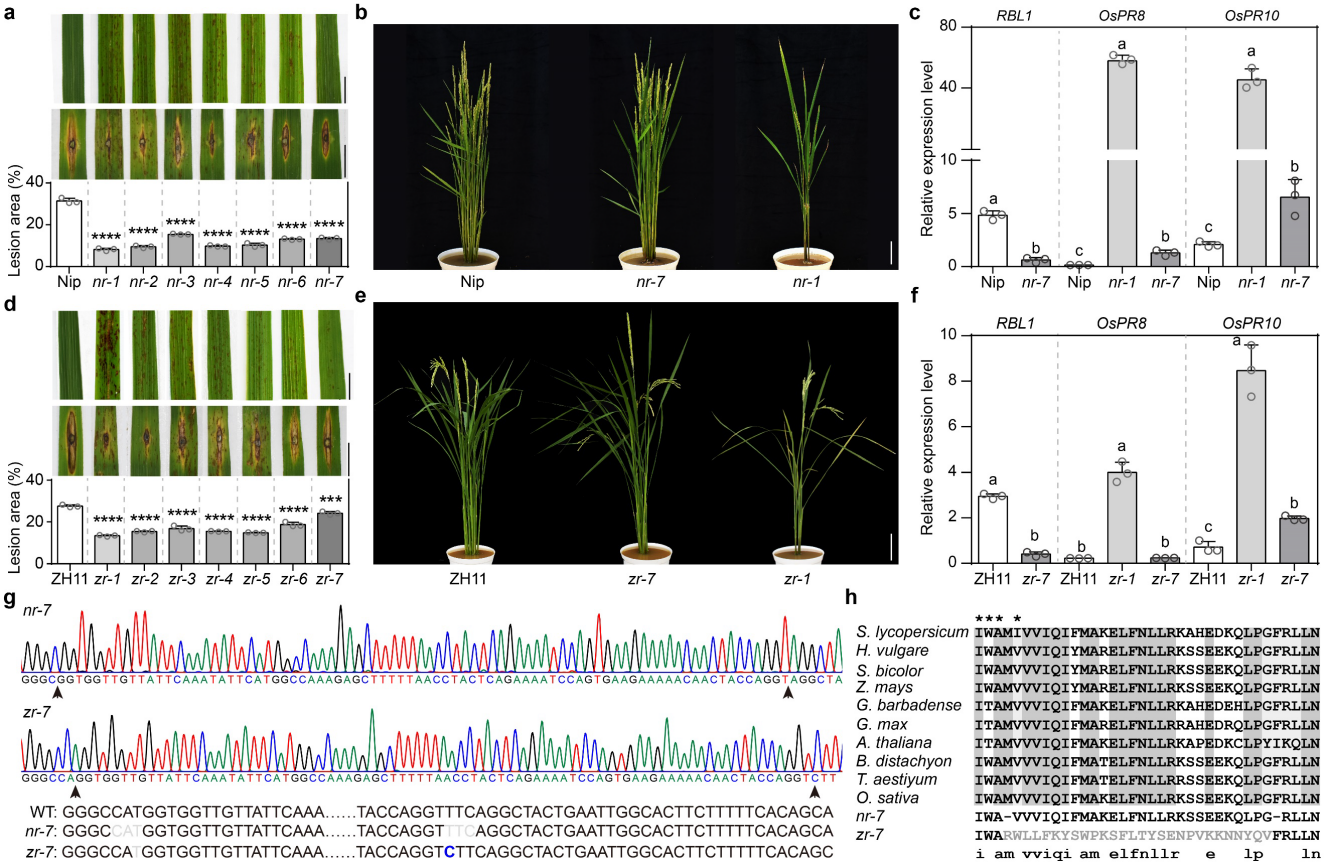

Extended Data Fig. 8 | Genome editing of *RBL1* enhances disease resistance in two other rice cultivars.

a, Lesion mimic phenotypes and enhanced resistance to *M. oryzae* in *RBL1*-edited Nipponbare (Nip) lines. Infected leaves and lesion area of punch-inoculated *RBL1*-edited lines with *M. oryzae* at 14 dpi. Bar, 1 cm. **b**, 12-week-old *RBL1*-edited Nipponbare lines. Bar, 10 cm. **c**, qRT-PCR assays of *RBL1* and plant defense-related genes *OsPR8* and *OsPR10* in the *RBL1*-edited Nipponbare lines. Total RNA was extracted from 4-week-old leaves. The *Actin* gene was used as the internal control. **d-f**, Similar assays as shown in (**a-c**) were performed on one local rice cultivar Zhonghua11 (ZH11). **g**, Sanger sequencing of the edited sites, indicated by arrows, in *nr-7* and *zr-7* lines, with the wild-type (WT, Kitaake) as the reference. The mutated nucleotides are shown in gray (deletion) and blue (insertion). **h**, Amino acid sequence alignment of the region mutated in lines *nr-7* and *zr-7*. The four amino acids truncated in RBL12 are indicated by asterisks. Shaded are conserved residues in the RBL1 homologs. Two amino acids are truncated in *nr-7*, with the first one overlapping the truncated region in RBL12. A 84-bp frameshift mutation caused by a 1-bp deletion followed by a 1-bp insertion alters the sequence of 28 amino acids (gray) in *zr-7*, with the first two overlapping the truncated region in RBL12. Bars indicate standard deviations, and asterisks indicate significant differences compared to the WT using the unpaired Student's *t*-test (***P < 0.001, ****P < 0.0001). Significant differences indicated by different letters in (**c**) and (**f**) were calculated using the Duncan's new multiple range test.